A Binocular Motor System Model and Its Application to Robot Eye Control

Xiaolin Zhang, Hidetoshi Wakamatsu, Member

Abstract In this paper, we propose a binocular motor system model from the viewpoint of systems and control engineering based on the anatomic structure and physiological function of the brainstem.Using the model, a unified transfer function is obtained for the different dynamic characteristics of conjugate and vergence eye movements including smooth pursuit, optokinetic response (OKR) and vestibulo-ocular reflex (VOR). Pairs of symmetrical coordinate systems are introduced to describe the kinematic and dynamic characteristics of the binocular movement, and account for the symmetrical structures and functions of the pairs of organs in the oculomotor system. A robot-eye system with a
control system similar to the model is described. The robot-eye system exhibits several characteristics specific to human-eye movement, including:
(1) Two-eye-one-point. Both eyes move in tandem and have the same target point in the central pits. This characteristic is considered as a basic condition for structuring a stereo-image using the image signals from both eyes.
(2) Moving together. That is to say, if one eye is shut or obstructed by an obstacle, the eye will follow the movement of the other eye so that it can find the target swiftly when the eye is opened or the obstacle is removed.
(3) Blur-compensation. The binocular motor system and the robot-eye system have the ability to compensate for the blurs caused by rotational and translational head movement.

Index Terms-- Robotics, Binocular motor system, Vestibulo-Ocular Reflex, Conjugate and Vergence eye movement, Smooth Pursuit.

I. INTRODUCTION

It is well known that the ocular motor control system is an effective device for capturing an object in the central pits of the retinas. The theoretical explanation of this control system principle has implications not only for medical science, but also for robotics, system control, image processing, etc.
In this paper the characteristics of the neural network in the brainstem for the oculomotor control system are analyzed through a mathematical model. Since the capacities of the cerebrum, cerebellum and superior colliculus are not considered, many characteristics of the oculomotor system cannot be discussed. However, to understand the whole oculomotor system, the ability and function of the neural network within the brainstem for oculomotor control should be considered first. In my opinion that many basic functions of eye movement are performed by the brainstem. Models of the portions of the cerebrum and cerebellum that impact the ocular motor system can be built upon the base model of the brainstem. For structure a unified mathematical model for analyzing the characteristics of ocular motor control, the concept of eye movement patterns have to clear up from the viewpoint of system and control engineering. The classification of eye movement patterns in physiology is based on the phenomena of eye movements in different environments. These classifications, however, are very difficult to use in control engineering. One reason for this is that eye movements are controlled by many types of signals, and the signal types are not easily distinguished by observing different natural eye movements. For example, in smooth pursuit the signals of the retinal errors (difference between fovea center and target point position projected on retina) and the signals of the retinal slip velocity (or call it as .retinal image velocity., difference between eye and target velocity) always work together when the target object is big enough. In discussions using a model of a single eye, we redefined the concepts of eye movement patterns according to the philosophy of systems and control engineering [55].
That is, smooth pursuit is the part of eye movement that occurs as a result of the retinal error signals, optokinetic response (OKR) follows from the signals of the retinal slip velocity, and vestibulo-

ocular response (VOR) follows from the head movement signals (from vestibular organs). In order to discuss the control system for binocular movements, in this paper, we have to consider how to define the concepts of conjugate and vergence eye movements from the viewpoint of system and control engineering. Vergence eye movements are commonly treated as members of a distinct subclass of eye movements along with saccade, smooth pursuit, optokinetic response, and VOR movements, according to their particular dynamic behavior. However from the viewpoint of kinematics and dynamics, eye movements can be broken into a pair movement types, conjugate and vergence eye movements, each of which includes conjugate or vergence versions of the other four movement subclasses. This concept is used to classify eye movements in this work. In this paper we consider fusional vergence to be a type of saccade, because, not only do the vergence and saccade have almost the same latencies (the time from showing the target to the beginning of the eye movement), and the vergence movements almost never occur without an associated saccade under natural conditions [9], [53], but also their control signals and neural pathways are all related to the superior colliculi [7], [27], [53]. The fact that they have the same latencies (or dead time) means the lengths of neural pathways of the control signals for fusional vergence and for saccade are the same. Also, the fact that the fusional vergence and the saccade always occur together suggests that they are a result of the same original signals or that the original signals are produced by same process. For the purposes of work like that presented here, it is probably safe to divide binocular eye movement into conjugate saccade and vergence saccade, conjugate VOR and vergence VOR, conjugate smooth pursuit and vergence smooth pursuit, and conjugate optokinetic response and vergence optokinetic response. Vergence smooth pursuit can be considered as a part of accommodative vergence. This is because, like smooth pursuit, accommodative vergence movements occur only when retinal images on the fovea and its surrounding area produce stimulation[43]. Even though when the target moves in depth, the blur of the retinal image is conspicuous and likely plays a role in controlling accommodative vergence [31], the retinal error signal of each eye also can be considered an important control signal for accommodative vergence eye movements, in addition to its role in controlling conjugate smooth pursuit. To ease discussion, the control loop of blur signals will not be considered in the proposed model, and the discussion of vergence smooth pursuit will also use the signals of retinal error.

The optical vergence movements in most modern research can be considered as fusional vergence, i.e. the vergence saccade. This is because the neural systems of superior colliculi were included in the ocular motor models, and in the experiments, the vergence movements were induced by the stimulation of off-foveal retinal images, such as changes in the gazing target [7], [22], [26], [27]. Since the nerves originating from the superior colliculus are not included in the proposed model, the vergence saccades are not taken into consideration. All of the signal pathways and transfer functions in this model have been confirmed by physiological or anatomical experiments. This work benefits from an accurate representation of the physiological mechanism. Because of the complexity of the ocular motor system, some simplifying assumptions are introduced here:

1) All the transfer functions in the ocular motor system model are considered as linear [14], [36]. 2) The time delays caused by the image processing in the visual cortex, the signal transmission in nerves and others are neglected. 3) To simplify discussion, we focus on the horizontal eye movement caused by target motion and/or passive head movement (except for eye-neck reflex). 4) In the model, we take into account the signals of the retinal error and the retinal slip velocity. However, the mechanism of signal processing in the visual cortex is not discussed. 5) The intelligence of the cerebrum, including synthetic inference, prediction and the influence of attention [52], is excluded.

The Most previous binocular motor models were for analyzing the characteristics of VOR[1], [13], [14], [46], and the Cova and Galiana had proposed a unified binocular model integrated vergence (in this paper, it is called saccadic vergence) and VOR [7], [8]. The binocular motor system model in this paper are for represent the nature of conjugate and vergence eye movements, including smooth pursuit, optokinetic response and VOR. Since VOR was found when the head moves in a linear acceleration [16], in this paper the model includes VOR mechanisms not only for head rotation (VOR-R) but

also for head translation (VOR-T, or otolith-ocular reflex [20]). For easy understanding by engineers and easy use in robotics, this model are structured according the rule of kinematics, dynamics, and systems and control engineering. To confirm the effectiveness of the model in duplicating human eye behavior, results of testing on a robot-eyes system that uses the same control system as the model are presented. Although the complexity of the real neural system for ocular motor control necessitates the several restrictions described above on the proposed model, the robot-eye system realizes several important basic characteristics of eye movements. For example, Human eyes, unlike such as chameleon eyes, cannot gaze at two different targets at one time. Instead, a human.s eyes can easily catch the same point of a subject in both central pits of retinal and use the symmetrical images from the two retinas to produce a stereovision space in the visual cortex. In this paper we call the ability to gaze at the same target point with both eyes simultaneously as .same point gazing tendency.. In my opinion this is one of the basic conditions for structuring a stereovision in the visual cortex.

II. NEURON PATHS FOR HORIZONTAL OCULOMOTOR SYSTEM

As shown in Fig. 1, We first construct a neural pathway system for horizontal eye movement based on previous studies [2], [7], [23], [24], [25], [40], [51]. The black circles with connecting lines represent the inhibitory neural fibers, and the white circles with connecting lines represent the excitatory neural fibers.

The input neural pathways of VN (vestibular nucleus) are as follows:

(1) The excitatory nerves from HSC (horizontal semicircular canal) and U&S (utricle and saccule) tie to the type I neurons.

(2) The neural pathway starting from the temporal side of the retina via Chiasma opticum merges with the pathway from the nasal retina of the other eye , then pursues two different routes. First route: lateral geniculate nucleus (LGN) → visual cortex, → dorsolateral pontine nucleus (DLPN) → Ventral paraflocculus (VPFL) → VN type II neurons. Second route: the nucleus of the optic tract (NOT) → nucleus reticularis tegmenti pontis (NRTP) → VN type II neurons. VN type II neurons and type I neurons are connected with inhibitory neural fibers. In this model, We did not include the neural pathway from the macular area of the retina.

The neural pathways from VN to the ocular muscles are as follows.

(1) The excitatory neuron axon from type I neurons of VN connects to: a) Type II neurons of VN in the other side ; b) oculomotor nucleus (OMN) → medial rectus ; c) abducens nucleus (AN) in the reverse side → lateral rectus in the reverse side , and from the AN to OMN through MLF (Medial longitudinal fasciculus) .

(2) The inhibitory neural pathways from type I neurons of VN connect to: a) Type I neuron in the reverse side VN ; b) AN ; c) OMN in the reverse side .

II. COORDINATE SYSTEMS FOR BINOCULAR MOTOR CONTROL

To explain the relationship between the movements of the head, eyes and vestibular organs, a precise definition of coordinate systems and signal vectors is necessary. Most of the coordinate systems defined in past research were selected for accurate measurements or for the explanation of physiological phenomena and anatomical structures. Such is true for the coordinate systems used to explain the relationship between the eyeballs and the semicircular canals [34], [39], [40], [49], as well as those used to explain the geometric relationship between the eyeball and the muscles [32], [48]. The effect of this distinct goal in defining the coordinate systems in this paper is that in order to ease the mathematical analysis, some normative assumptions are made, even though these assumptions are not completely consistent with the facts of physiology and anatomy. This includes, for example, assuming that the

semicircular canals are perpendicular to each other, that the lateral canal planes are parallel to the plane of the macula of utricles, that the target is far enough away compared to the radius of the eyeball, etc. Of course, making such assumptions risks losing some information specific to the organ.s own structures.

As shown in Fig. 1, both the configuration of the neural pathways and the structure of vestibular organs and retinas are symmetrical with respect to the midline. This means that when the head rotates in one direction, the output signals from one side of the horizontal canal, utricle and saccule are the reverse of the signals from the other side. Similar to vestibular organs, retinas also are composed of a nasal side and temporal side. Therefore, pairs of symmetrical coordinate systems are defined for the pairs of the organs.

A. Coordinate system for vestibular organs

As is well known, semicircular canals are sensors for head rotation, and utricles and saccule are sensors for head translation. Their anatomic structures are shown in Fig. 2.

The vectors on the maculae of the utricle and saccule represent the directions of stimuli that cause the hair cell to fire [47]. When the head tilts approximately 30 degrees forward from the upright position, the lateral ductus and utricular maculae lie in the horizontal plane and the saccules maculae in the sagittal plane [2], [23].

The horizontal movement of head and eyeballs is discussed under the assumption that the head is tilted 30 degrees forward. According to the anatomical structure of the utricle and saccule, utricles are for the measurement of horizontal translation, and saccules are for the measurement of sagittal plane translation [10], [47]. To eliminate the influence of centrifugal force, due to rotations around its own axes in the coordinate system of vestibular organ, the axis of the coordinates has to be defined in parallel to the planes of maculae or through the center of the gravity of the maculae. Thence, the vertical axis (*zV*-axis) is set through the center of gravity of the utricle macula. The *yV*-axis is parallel to the plane of the utricle macula and through the center of gravity of the saccule macula, and crosses the *zV*-axis. The *xV*-axis is set through the crossing point *OV* and perpendicular to the *yV-zV* plane. So, the coordinate systems for the otoliths are defined as shown in Fig. 2, where *OV* is the origin. Since semicircular canals respond only to rotational acceleration, the signals of the nerves from the ampullae of the canal (i.e. the results measured by the canal), respond only to the component of head rotation around the axis perpendicular to the plane of the canal. Since the three semicircular canals are almost perpendicular to each other, head rotation is measured in three-dimensional space. Here, We assume the semicircular canals are perpendicular to each other. The coordinate systems for the semicircular canals *xs- ys-zs* are defined as shown in

Fig. 2, where the axes x_s, y_s and z_s are vertical to the anterior ductus plane, posterior ductus plane and lateral ductus plane, respectively. Since semicircular canals respond only to rotational head movements, the locations of the coordinate system origins do not influence the measurement results with the coordinates defined this way. So, the origins of the coordinate systems are set to coincide with O_V, the origins of the coordinate systems for the otoliths. Here We assume that (1) the x_V-axis is parallel to both the plane of the macula of utricle and saccule plane, (2) the distances from the origin of the coordinate system for the vestibular organ O_V to the macula planes of utricle and saccule are short enough. (3) The plane of the lateral ductus is parallel to the plane of the macula of utricle, i.e. the axes z_S and z_V overlap each other. Since only horizontal head movement is discussed here, the coordinate systems for the vestibular organs will only be used for translation in the x_v and y_v axis directions and the rotations around the z_s or z_v axis. When the head rotates counterclockwise (to the left), the discharge rate of the left vestibular neuron from the lateral canal becomes higher, while the rate of the right one becomes lower [2], [16], [38]. Therefore, counterclockwise is positive rotation in the left vestibular coordinate system, and clockwise is positive rotation in the right vestibular coordinate system.

Since the directions of the stimuli that cause the hair cells to ignite are reversed on each side of crest striola [47], all directions of acceleration on the plane of the macula are detectable. The effects of the signals from the hair cells on the vestibular nucleus depend on the synaptic transmission gains. The axes of the coordinate systems are defined as in Fig. 2 (a)(b).

B. Coordinate system for eyeballs

In the ocular motor system, eyeballs are not only controlled objects but also sensors for detecting the position and velocity of the target. In Section II, We mentioned that a retina can be divided into a nasal side and temporal side, on the basis of its physiological structure. The coordinate systems of eyeballs also have to be defined as a pair of symmetrical coordinate systems.

Corresponding to the vestibular coordinate systems, the eyeball fixed coordinate systems (x_E-y_E) and orbit fixed coordinate systems (x_O-y_O) are defined as in Fig. 3. The origins of both coordinate systems are defined on the rotational center of the eyeball *OE*. The axis *xE* is defined to be parallel to the optical line. The axis x_O is defined so that it coincides with *xE* when the eyeball looks at a target infinitely far ahead. When the target is at point *Tg*, *R* (rad) is the angle that the target projects on the retina, namely the angle between the optical line and O_L-*Tg*, where *OL* is the principal point of the lens. *.et* (rad) is the angle between the optical line and line O_E-*Tg*, *.oe* (rad) is the angle between the axis x_O and *xE*, and *.ot* (rad) is the angle between the axis x_O and line *OE-Tg*. Since the axis *xE* is parallel with the optical line, *.et* is also the angle between the axis *xE* and line *OE-Tg*. When the distance of the target *ret* is far enough compared with the radius of the eyeball *re*, *.et* can be considered to be equal to *R*. Therefore, in an ocular motor control system, *.oe* (rad), *.ot* (rad), and *R* or *.et* are the controlled variable, desired value, and controlled error, respectively.

So that the positive rotation of eyeball fixed coordinates and head translation in the y_E axis direction have the same visual effect on the retina, we define the counterclockwise rotation of the left eyeball fixed coordinate system and the clockwise rotation of the right eyeball fixed coordinate system to be positive. Accordingly, the contracted force of the lateral rectus muscle is a positive manipulated variable, and the contracted force of the medial rectus muscle is a negative one.

C. Coordinate system for head and target

Fig. 4 shown the base and head fixed coordinate systems. A base plane can be defined as having all the origins of coordinate systems. Here, the two origins of vestibular coordinates, the two origins of orbit fixed coordinates and the origin of the head fixed coordinate system are all on the base plane. The origin of the head-fixed coordinate system (x_H-y_H) is defined at the middle point of the line that connects $O_{V\text{-}l}$ and $O_{V\text{-}r}$, the origins of left and right vestibular coordinate systems. The y_H-axis of the head-fixed coordinate system is defined on the line connecting $O_{V\text{-}l}$ and $O_{V\text{-}r}$. Before the head moves, the head-fixed coordinate system coincides with the base coordinate system. A counterclockwise direction is defined as the positive rotational direction.

As shown in Fig. 4, $.h_b$ is the head rotation angle. $.h_t$ represents the angle between the line O_H-*Tg* and the *xH* axis. *xhb* and *yhb* represent the translation distances of the head in *xB* and *yB* directions. And *xt* and *yt* represent the translation distances of target point *Tg* in x_B and y_B directions. r_{hv} represents the distance between O_H and $O_{V\text{-}l}$ or $O_{V\text{-}r}$, *rhe* the distance between O_H and $O_{E\text{-}l}$ or $O_{E\text{-}r}$, and *.he* the angle between the line O_H - $O_{E\text{-}l}$ ($O_{E\text{-}r}$) and x_H axis.

D. Transformation of binocular coordinate systems

As shown in Fig. 4, the head motion vectors are:

$$\boldsymbol{H}(t) = \begin{bmatrix} x_{hb}(t) & y_{hb}(t) & \varphi_{hb}(t) \end{bmatrix}^T \quad (1)$$

$$\dot{\boldsymbol{H}}(t) = \begin{bmatrix} \dot{x}_h(t) & \dot{y}_h(t) & \dot{\varphi}_h(t) \end{bmatrix}^T \quad (2)$$

$$\ddot{\boldsymbol{H}}(t) = \begin{bmatrix} \ddot{x}_h(t) & \ddot{y}_h(t) & \ddot{\varphi}_h(t) \end{bmatrix}^T \tag{3}$$

Here, $\dot{x}_h(t)$ and $\dot{y}_h(t)$ represent the translation velocities (m/s) of the head in the x_H and y_H directions, and $\dot{\varphi}_h(t)$ is the rotational velocity (rad/s) of the head around O_H. $\ddot{x}_h(t)$, $\ddot{y}_h(t)$ and $\ddot{\varphi}_h(t)$ are the accelerations. The target point position and its velocity are:

$$\boldsymbol{T}_g(t) = \begin{bmatrix} x_t(t) & y_t(t) \end{bmatrix}^T \tag{4}$$

$$\dot{\boldsymbol{T}}_g(t) = \begin{bmatrix} \dot{x}_t(t) & \dot{y}_t(t) \end{bmatrix}^T \tag{5}$$

Since vestibular organs respond only to accelerations, the acceleration vectors of the left and right vestibular organs shown in Fig. 2 and 4 are as follows:

$$\begin{aligned} \ddot{\boldsymbol{V}}_l(t) &= \begin{bmatrix} \ddot{x}_{v-l}(t) & \ddot{y}_{v-l}(t) & \ddot{\varphi}_{v-l}(t) \end{bmatrix}^T \\ &= \begin{bmatrix} \ddot{x}_h(t) - r_{hv}\ddot{\varphi}_h(t) & \ddot{y}_h(t) + r_{hv}\dot{\varphi}_h^2(t) & \ddot{\varphi}_h(t) \end{bmatrix}^T \end{aligned} \tag{6}$$

$$\begin{aligned} \ddot{\boldsymbol{V}}_r(t) &= \begin{bmatrix} \ddot{x}_{v-r}(t) & \ddot{y}_{v-r}(t) & \ddot{\varphi}_{v-r}(t) \end{bmatrix}^T \\ &= \begin{bmatrix} \ddot{x}_h(t) + r_{hv}\ddot{\varphi}_h(t) & -\ddot{y}_h(t) + r_{hv}\dot{\varphi}_h^2(t) & -\ddot{\varphi}_h(t) \end{bmatrix}^T \end{aligned} \tag{7}$$

$\ddot{x}_{v-l}(t)$ and $\ddot{y}_{v-l}(t)$ represent the accelerations of the left vestibular organ in the $x_{V\text{-}l}$ and $y_{V\text{-}l}$ axes and $\ddot{\varphi}_{v-l}(t)$ the rotational acceleration around $O_{V\text{-}l}$. $\ddot{\boldsymbol{V}}_r(t)$ is the acceleration vector of the right vestibular organ. Here $r_v\dot{\varphi}_h^2(t)$ is the centrifugal acceleration of the origin of the coordinate system of a vestibular organ caused by head rotation around O_H.

As shown in Fig. 3 (a)(b), the following equations can be obtained:

$$\varphi_{oe-l}(t) + \varphi_{et-l}(t) = \varphi_{ot-l}(t) \tag{8}$$

$$\varphi_{oe-r}(t) + \varphi_{et-r}(t) = \varphi_{ot-r}(t) \tag{9}$$

Using Fig. 4, the desired values of the eyeballs are given as:

$$\varphi_{et-l}(t) = -\varphi_{hh}(t) + \tan^{-1}\frac{y_t(t) - y_{hh}(t) - r_{he}\sin(\varphi_{hh}(t) + \varphi_{he})}{x_t(t) - x_{hh}(t) - r_{he}\cos(\varphi_{hh}(t) + \varphi_{he})} \tag{10}$$

$$\varphi_{et-r}(t) = \varphi_{hh}(t) - \tan^{-1}\frac{y_t(t) - y_{hh}(t) - r_{he}\sin(\varphi_{hh}(t) - \varphi_{he})}{x_t(t) - x_{hh}(t) - r_{he}\cos(\varphi_{hh}(t) - \varphi_{he})} \tag{11}$$

IV. CHARACTERISTICS OF SIGNAL PROCESSING AND TRANSMISSION OF ELEMENTS IN OCULAR MOTOR SYSTEM

A. Transfer function of vestibular organ

The outputs from the canal, saccule and utricle are considered as the firing rates of primary fibers. The variation of the steady values of the firing rates from the resting rates of each canal, saccule and utricle of a vestibular organ are nearly linear to the accelerations of rotation and translation, respectively [10], [16]. So, We define the signal values of the resting rates of the primary fibers of the canal, saccule and utricle to be 0 (imp./s). For all the neuron fibers that have a resting rate other than 0, the firing rate minus the resting rate is used.

The transfer function of the semicircular canal is documented in past research [14], [16], and can be expressed by:

$$\omega_s(s) = \frac{g_s T_s}{T_s s + 1}\ddot{\varphi}_h(s) \tag{12}$$

where $\omega(t)$ (imp./s) is the output from the semicircular canal, T_s (sec) is the time constant, and g_s (imp.s^{-1}/rad s^{-2}) is the gain or sensitivity of the firing rate modulation on the canal primary fibers with

respect to head rotation.

In contrast to the semicircular canal, primary otolith afferents carry a signal that remains approximately in phase with and linear to head acceleration in the same frequency range [11], [12]. Thus from the viewpoint of control engineering, two integrations of the otolith signal are required to produce the appropriate compensatory ocular displacement during translation. This idea is hypothesized in the literature [18], [33], [35], [50]. Furthermore, all current hypotheses for otolith processing agree that one integration is performed by the neural integrator[41] which is shared with the rotational system [18]. Little is known about how and where the second integration is processed. In my opinion that this second integration is likely to be found to be a result of the signal processing characteristics of individual neurons. Most neurons have both fast and slow neurotransmitters, and the time constants of slow postsynaptic potential caused by slow neurotransmitters are from several seconds to several minutes [19], [21]. This means that the effect of a pulse from the synapse might remain for minutes and could be added to subsequent input pulses. It is clear that the slow neurotransmitters might be related to the integral behavior. We will discuss the details of the signal processing behavior of neurons in another paper. To ease understanding, in this paper we also represent the dynamics from an otolith to a vestibular nucleus with a transfer function similar to that for the semicircular canal. However the time constant is far smaller than that for the semicircular canals [18]. Thus the saccule and utricle are described by the following equations:

$$v_{vx}(s) = \frac{g_v T_v}{T_v s + 1} \ddot{x}_v(s) \tag{13}$$

$$v_{vy}(s) = \frac{g_v T_v}{T_v s + 1} \ddot{y}_v(s) \tag{14}$$

where $v_{vx}(t)$ and $v_{vy}(t)$ (imp./s) are the outputs from the saccule or utricle, responding to the head movement in the *x*-axis and *y*-axis directions, respectively. T_v (sec) is the time constant of the transfer functions for the saccule and utricle, g_v (imp.s^{-1}/m.s^{-2}) represents the gain or sensitivity of the firing rate modulation on the saccule and utricle primary fibers with respect to head translation accelerations. To ease analysis, we assume that the transfer functions from the saccule to the vestibular nucleus and from the utricle to the vestibular nucleus are the same. Furthermore the gain g_v , which has been detected as variable depending on the distance to the target in physiological experiments [3], is considered constant here.

B. Transfer function of neural pathways from vestibular nucleus to ocular motor nucleus. The transfer function of the neural pathways from the vestibular nucleus to the abducens nucleus or the oculomotor nucleus can be expressed as the sum of an imperfect integrator and a direct path [4], [5], [36], [38], [41], [44], [45]. That is:

$$G_{vm}(s) = \frac{g_{vmi} T_{vm}}{T_{vm} s + 1} + g_{vmd} \tag{15}$$

where T_{vm} (sec) is the time constant of the integrator, and g_{vmi} and g_{vmd} (dimensionless) are the gains of the integral pathway and the direct path.

The principle and the structure of the neural integrator is not clear. It has been thought that the location is in the vicinity of the complex formed by the nucleus prepositus hypoglossi and the medial vestibular nucleus [29] and the dynamics have been represented using low pass filters [7], [14]. As mentioned above, we also think the neural integrator is only one of the characteristics of signal processing of neurons, and is related to the slow neurotransmitters of the neuron. The neural integrator is not explicitly represented by any structure in Fig. 1.

In this paper, it is enough to know that there is an integrator between the vestibular nucleus and the motor nucleus.

To simplify the mathematical analysis, we assume that all the neural pathways from vestibular nucleus to

motor nucleus have the same transfer function as equation (15). From equation (15), the following equation can be obtained:

$$G_{vm}(s) = g_{vm} T_{vm} \frac{T_d s + 1}{T_{vm} s + 1} \tag{16}$$

where,

$$T_d = \frac{g_{vmd} T_{vm}}{g_{vmi} T_{vm} + g_{vmd}}, \quad g_{vm} = \frac{g_{vmi} T_{vm} + g_{vmd}}{T_{vm}}$$

C. Transfer function of eye plant.

The dynamics of an eye plant have described by a viscoelastic model [36], and in most ocular motor models the eye plant is represented as a first order delay system. To permit easy understanding of the dynamic characteristics of an eyeball, a new viscoelastic model to explain the eye plant is proposed and shown in Fig. 5(b). The model is based on the anatomical structure of Fig. 5(a). In this model, k_{sl} and k_{sm} (N/m) are the coefficients of elasticity, k_{dl} , k_{dm} (N/m•s^{-1}) are the coefficients of viscosity of the lateral and medial rectus muscles, $F_l(t)$ and $F_m(t)$ (N) are the forces generated by lateral and medial rectus muscles, m (kg) represents the mass of the equivalent ring, and re is the radius of the eyeball. As shown in Fig. 5(b), the rotational angle of the eyeball $\varphi_{oe}(s)$ (rad) can be approximated by the following equation:

$$\varphi_{oe}(s) = \frac{F_l(s) - F_m(s)}{m r_e s^2 + (k_{dl} + k_{dm}) r_e s + (k_{sl} + k_{sm}) r_e} \tag{17}$$

If the effect of the eyeball.s mass is small enough compared with the elasticity and viscosity in the equation (17), the transfer function of the controlled object is:

$$\varphi_{oe}(s) = \frac{F_l(s) - F_m(s)}{(k_{sl} + k_{sm}) r_e \left(\frac{k_{dl} + k_{dm}}{k_{sl} + k_{sm}} s + 1 \right)} \tag{18}$$

From equation (18) we have

$$\varphi_{oe}(s) = \frac{1}{T_e s + 1} \left(g_m C_o(s) - g_l C_a(s) \right) \tag{19}$$

where,

$$T_e = \frac{k_{dl} + k_{dm}}{k_{sl} + k_{sm}}, \quad F_l(s) = \delta_l C_l(s), \quad F_m(s) = \delta_m C_m(s), \quad g_l = \frac{\delta_l}{r_e (k_{sl} + k_{sm})}, \quad g_m = \frac{\delta_m}{r_e (k_{sl} + k_{sm})}$$

Te (sec) is the time constant. δ_1 and δ_m (N/imp.s^{-1}) are the gains of the forces $F_l(t)$ and $F_m(t)$ (N) due to ocular muscle modulation on the fibers from the abducens nucleus and ocular motor nucleus. These forces are proportional to the firing rates C_l(t) and C_m(t) (imp.s^{-1}).

The same characteristics of (19) have been shown in experiments on monkeys performed by Skavensky and Robinson [45], and similar transfer functions are used in most ocular motor system models.

D. Linearization of the characteristics of the nucleus

In this paper, we only consider the linear characteristics of the ocular motor system. According to past research, we can assume the nucleus to be an addition device as shown in Fig. 6 that is, the outputs of the nucleus are the sum of the input values [37], [42]. Therefore

$$O_m(t) = \sum k_{p,j} I_{p,j}(t) - \sum k_{n,j} I_{n,j}(t) \tag{20}$$

$O_m(t)$ is the number m output neuron fiber's firing rate (imp./s). $I_{p,i}(t)$ is the firing rate (imp./s) of the number *i* excitatory input neuron fiber connected to the neurons whose axons are included in the number m output fiber. Similarly, $I_{n,j}(t)$ is the firing rate (imp./s) of the number j inhibitory input neuron fiber connected to the neurons whose axons are included in the number m output fiber. $k_{p,i}$ and $k_{n,j}$ are the synaptic transmission gains. All the gains $k_{p,i}$ (i=1,2,3, ...) and $k_{n,j}$ (j=1,2,3, ...) in equation (20) are positive. The approach of Fig. 6 and (20) is not exclusive to the modeling of neural systems, and is here only arranged to represent the nucleus dynamics in a clean way. Fig. 6 and (20) are similar to a unit of the neural network back-propagation model proposed by Rumelhart, Hinton, and Williams (1986), when only the linear part of the sigmoid function is considered [42].

V. MODELING AND ANALYSIS OF BINOCULAR MOTOR SYSTEM

Using the information established in the last section, the binocular motor system shown in Fig. 1 can be explained using a block diagram as shown in Fig. 7, where α, β, γ represent the synaptic transmission gains of vestibular, abducent and oculomotor nuclei, respectively. Since the eyeball fixed coordinate systems are symmetrical with respect to the midline, the retinal signals transformed to the reverse vestibular nucleus have to be multiplied by -1.

When $T_d = T_e$, the denominator of the ocular muscle transfer function can be canceled [38], [55]. Fig. 8 is obtained by rearranging the block diagram of Fig. 7. Then, unify the parameters in Fig. 8, and the simple block diagram of the oculomotor control system is obtained as shown in Fig. 9, where

$$\sigma = \alpha_3\alpha_5,\ \eta = \alpha_3\alpha_6,\ \sigma_r = \alpha_3\alpha_7,\ \eta_r = \alpha_3\alpha_8,$$

$$\rho = \frac{g_{vm}}{1-(\alpha_1+\alpha_3\alpha_2)^2}\left(g_l\beta_1 + g_m\gamma_1 + g_m\beta_2\gamma_3\right),\quad \rho_r = \frac{g_{vm}}{1-(\alpha_1+\alpha_3\alpha_2)^2}\left(g_l\beta_2 + g_w\gamma_2 + g_m\beta_1\gamma_3\right),$$

$$\kappa_x = g_v\alpha_{1x},\ \kappa_y = g_v\alpha_{1y},\ \kappa_\varphi = g_s\alpha_{1\varphi},\ \kappa_{xr} = g_v\alpha_{1xr},\ \kappa_{yr} = g_v\alpha_{1yr},\ \kappa_{\varphi r} = g_s\alpha_{1\varphi r}$$

From Fig. 9, the following equations are obtained:

$$\begin{aligned}
\varphi_{oe-l}(s) = {} & -\rho\frac{T_{vm}}{T_{vm}s+1}\left[\kappa_x\frac{T_v}{T_vs+1}\ddot{x}_{v-l}(s) + \kappa_y\frac{T_v}{T_vs+1}\ddot{y}_{v-l}(s) + \kappa_\varphi\frac{T_s}{T_ss+1}\ddot{\varphi}_{v-l}(s) - \kappa_{xr}\frac{T_v}{T_vs+1}\ddot{x}_{v-r}(s) - \kappa_{yr}\frac{T_v}{T_vs+1}\ddot{y}_{v-r}(s) - \kappa_{\varphi r}\frac{T_s}{T_ss+1}\ddot{\varphi}_{v-r}(s)\right] \\
& -\rho\frac{T_{vm}}{T_{vm}s+1}\left[-(\sigma+\eta s)(\varphi_{ot-l}(s)-\varphi_{oe-l}(s)) + (\sigma_r+\eta_r s)(\varphi_{ot-r}(s)-\varphi_{oe-r}(s))\right] \\
& +\rho_r\frac{T_{vm}}{T_{vm}s+1}\left[\kappa_x\frac{T_v}{T_vs+1}\ddot{x}_{v-r}(s) + \kappa_y\frac{T_v}{T_vs+1}\ddot{y}_{v-r}(s) + \kappa_\varphi\frac{T_s}{T_ss+1}\ddot{\varphi}_{v-r}(s) - \kappa_{xr}\frac{T_v}{T_vs+1}\ddot{x}_{v-l}(s) - \kappa_{yr}\frac{T_v}{T_vs+1}\ddot{y}_{v-l}(s) - \kappa_{\varphi r}\frac{T_s}{T_ss+1}\ddot{\varphi}_{v-l}(s)\right] \\
& +\rho_r\frac{T_{vm}}{T_{vm}s+1}\left[-(\sigma+\eta s)(\varphi_{ot-r}(s)-\varphi_{oe-r}(s)) + (\sigma_r+\eta_r s)(\varphi_{ot-l}(s)-\varphi_{oe-l}(s))\right]
\end{aligned} \tag{21}$$

$$\begin{aligned}
\varphi_{oe-r}(s) = {} & -\rho\frac{T_{vm}}{T_{vm}s+1}\left[\kappa_x\frac{T_v}{T_vs+1}\ddot{x}_{v-r}(s) + \kappa_y\frac{T_v}{T_vs+1}\ddot{y}_{v-r}(s) + \kappa_\varphi\frac{T_s}{T_ss+1}\ddot{\varphi}_{v-r}(s) - \kappa_{xr}\frac{T_v}{T_vs+1}\ddot{x}_{v-l}(s) - \kappa_{yr}\frac{T_v}{T_vs+1}\ddot{y}_{v-l}(s) - \kappa_{\varphi r}\frac{T_s}{T_ss+1}\ddot{\varphi}_{v-l}(s)\right] \\
& -\rho\frac{T_{vm}}{T_{vm}s+1}\left[-(\sigma+\eta s)(\varphi_{ot-r}(s)-\varphi_{oe-r}(s)) + (\sigma_r+\eta_r s)(\varphi_{ot-l}(s)-\varphi_{oe-l}(s))\right] \\
& +\rho_r\frac{T_{vm}}{T_{vm}s+1}\left[\kappa_x\frac{T_v}{T_vs+1}\ddot{x}_{v-l}(s) + \kappa_y\frac{T_v}{T_vs+1}\ddot{y}_{v-l}(s) + \kappa_\varphi\frac{T_s}{T_ss+1}\ddot{\varphi}_{v-l}(s) - \kappa_{xr}\frac{T_v}{T_vs+1}\ddot{x}_{v-r}(s) - \kappa_{yr}\frac{T_v}{T_vs+1}\ddot{y}_{v-r}(s) - \kappa_{\varphi r}\frac{T_s}{T_ss+1}\ddot{\varphi}_{v-r}(s)\right] \\
& +\rho_r\frac{T_{vm}}{T_{vm}s+1}\left[-(\sigma+\eta s)(\varphi_{ot-l}(s)-\varphi_{oe-l}(s)) + (\sigma_r+\eta_r s)(\varphi_{ot-r}(s)-\varphi_{oe-r}(s))\right]
\end{aligned} \tag{22}$$

If we respectively add and subtract (21) and (22), the following equations are obtained:

$$\varphi_{oe-l}(s)+\varphi_{oe-r}(s)=\frac{T_{vm}(\rho-\rho_r)}{1+T_{vm}(\rho-\rho_r)(\sigma-\sigma_r)+T_{vm}(1+(\rho-\rho_r)(\eta-\eta_r))s}$$
$$\times\left[-(\kappa_x-\kappa_{xr})\frac{T_v}{T_vs+1}(\ddot{x}_{v-l}(s)+\ddot{x}_{v-r}(s))-(\kappa_y-\kappa_{yr})\frac{T_v}{T_vs+1}(\ddot{y}_{v-l}(s)+\ddot{y}_{v-r}(s))\right.$$
$$\left.-(\kappa_\varphi-\kappa_{\varphi r})\frac{T_s}{T_ss+1}(\ddot{\varphi}_{v-l}(s)+\ddot{\varphi}_{v-r}(s))+(\sigma-\sigma_r)(\varphi_{ot-l}(s)+\varphi_{ot-r}(s))+(\eta-\eta_r)(\dot{\varphi}_{ot-l}(s)+\dot{\varphi}_{ot-r}(s))\right]$$

(23)

$$\varphi_{oe-l}(s)-\varphi_{oe-r}(s)=\frac{T_{vm}(\rho+\rho_r)}{1+T_{vm}(\rho+\rho_r)(\sigma+\sigma_r)+T_{vm}(1+(\rho+\rho_r)(\eta+\eta_r))s}$$
$$\times\left[-(\kappa_x+\kappa_{xr})\frac{T_v}{T_vs+1}(\ddot{x}_{v-l}(s)-\ddot{x}_{v-r}(s))-(\kappa_y+\kappa_{yr})\frac{T_v}{T_vs+1}(\ddot{y}_{v-l}(s)-\ddot{y}_{v-r}(s))\right.$$
$$\left.-(\kappa_\varphi+\kappa_{\varphi r})\frac{T_s}{T_ss+1}(\ddot{\varphi}_{v-l}(s)-\ddot{\varphi}_{v-r}(s))+(\sigma+\sigma_r)(\varphi_{ot-l}(s)-\varphi_{ot-r}(s))+(\eta+\eta_r)(\dot{\varphi}_{ot-l}(s)-\dot{\varphi}_{ot-r}(s))\right]$$

(24)

Equation (2 presents the functions of vergence movements, and equation (24) of conjugate movements. If we respectively add and subtract (23) and (24), and using equations (6), (7) the following equation is obtained

$$\begin{bmatrix}\varphi_{oe-l}(s)\\ \varphi_{oe-r}(s)\end{bmatrix}=\frac{T_{vm}(\rho-\rho_r)}{1+T_{vm}(\rho-\rho_r)(\sigma-\sigma_r)+T_{vm}(1+(\rho-\rho_r)(\eta-\eta_r))s}$$
$$\times\left(-(\kappa_x-\kappa_{xr})\frac{T_v}{T_vs+1}\ddot{x}_h(s)-(\kappa_y-\kappa_{yr})\frac{T_v}{T_vs+1}r_{hv}\dot{\varphi}_h^2(s)\right.$$
$$\left.+\frac{1}{2}(\sigma-\sigma_r)(\varphi_{ot-l}(s)+\varphi_{ot-r}(s))+\frac{1}{2}(\eta-\eta_r)(\dot{\varphi}_{ot-l}(s)+\dot{\varphi}_{ot-r}(s))\right)\begin{bmatrix}1\\1\end{bmatrix}$$
$$+\frac{T_{vm}(\rho+\rho_r)}{1+T_{vm}(\rho+\rho_r)(\sigma+\sigma_r)+T_{vm}(1+(\rho+\rho_r)(\eta+\eta_r))s}$$
$$\times\left((\kappa_x+\kappa_{xr})\frac{T_v}{T_vs+1}r_{hv}\ddot{\varphi}_h(s)-(\kappa_y+\kappa_{yr})\frac{T_v}{T_vs+1}\ddot{y}_h(s)-(\kappa_\varphi+\kappa_{\varphi r})\frac{T_s}{T_ss+1}\ddot{\varphi}_h(s)\right.$$
$$\left.+\frac{1}{2}(\sigma+\sigma_r)(\varphi_{ot-l}(s)-\varphi_{ot-r}(s))+\frac{1}{2}(\eta+\eta_r)(\dot{\varphi}_{ot-l}(s)-\dot{\varphi}_{ot-r}(s))\right)\begin{bmatrix}1\\-1\end{bmatrix}$$

(25)

Here, $\dot{\varphi}_h^2(s)$ represents the Laplace transform of the square of $\dot{\varphi}_h(t)$ i.e. $\dot{\varphi}_h^2(s)=\mathcal{L}\left[(\dot{\varphi}_h(t))^2\right]$, and the term including $\dot{\varphi}_h^2(s)$ represents the influence of centrifugal acceleration.

Here we assume that smooth pursuit is the part of eye movement that is induced by the retinal error signals, optokinetic response by the signals of the retinal slip velocity, and VOR by the head movement signals (from vestibular organs) [55]. So, the terms of equation (25) that include $\ddot{x}_h(s)$ and $\dot{\varphi}_h^2(s)$ represent the effects of vestibular ocular reflexes of vergence movement, those that include $\ddot{y}_h(s)$ and

$\ddot{\varphi}_h(s)$ represent the effects of vestibular ocular reflexes of conjugate movement, the terms that include $(\varphi_{ot-l}(s)+\varphi_{ot-r}(s))$ show smooth pursuit of vergence movement, and those with $(\varphi_{ot-l}(s)-\varphi_{ot-r}(s))$ show the smooth pursuit of conjugate movement. $(\dot{\varphi}_{ot-l}(t)+\dot{\varphi}_{ot-r}(t))$ is the function describing optokinetic response of vergence, and $(\dot{\varphi}_{ot-l}(t)-\dot{\varphi}_{ot-r}(t))$ is the function of optokinetic response of conjugate movement.

From equation (25) it is clear that except for the function of each sensor (semicircular canal, otolith and retinal), all types of vergence eye movements have the same transfer function

$$\frac{T_{vm}(\rho-\rho_r)}{1+T_{vm}(\rho-\rho_r)(\sigma-\sigma_r)+T_{vm}(1+(\rho-\rho_r)(\eta-\eta_r))s} \tag{26}$$

Similarly, all types of conjugate eye movements also have the same transfer function:

$$\frac{T_{vm}(\rho+\rho_r)}{1+T_{vm}(\rho+\rho_r)(\sigma+\sigma_r)+T_{vm}(1+(\rho+\rho_r)(\eta+\eta_r))s} \tag{27}$$

When $\rho = \rho_r$ the transfer function of vergence will become 0; in this case all types of vergence eye movements will disappear. In the case of $\sigma = \acute{o}_r$, the smooth pursuit of vergence will disappear, and if $\eta = \eta_r$,optokinetic response of vergence will disappear. If $\kappa_y = \kappa_{yr}$, the influence of centrifugal acceleration on vergence movement will disappear. In earlier work we discussed the influence of centrifugal acceleration in the pathological case [54], but even in normal eye movement, the influence of centrifugal acceleration will interfere with gazing. Throughout this paper, we consider the case when $\kappa_y = \kappa_{yr}$, so that the centrifugal acceleration will not be considered.

Since all the parameters in Fig. 9 are positive (see Section IV.D), the poles of the conjugate eye movement transfer function are always negative, and the conjugate eye movement is always stable. The necessary conditions for stability of vergence eye movements are obtained from (26) as shown in the following:

$$\frac{1+T_{vm}(\rho-\rho_r)(\sigma-\sigma_r)}{T_{vm}(1+(\rho-\rho_r)(\eta-\eta_r))}>0 \tag{28}$$

In normal vestibular reflex, if the head translates forward, convergence will occur, and if the head translates back, divergence will occur. The smooth pursuit vergence and optokinetic response vergence also consider relative motion between the target and the eyes. To ease application to robotics, the following sufficient condition for the system stability is useful for parameter setting:

$$\sigma>\sigma_r,\ \rho>\rho_r,\ \eta>\eta_r,\ \kappa_x>\kappa_{xr},\kappa_y=\kappa_{yr} \tag{29}$$

The time constant of (26) is

$$T_{vergence}=\frac{T_{vm}+T_{vm}(\rho-\rho_r)(\eta-\eta_r)}{1+T_{vm}(\rho-\rho_r)(\sigma-\sigma_r)} \tag{30}$$

The time constant of (27) is

$$T_{conjugate}=\frac{T_{vm}+T_{vm}(\rho+\rho_r)(\eta+\eta_r)}{1+T_{vm}(\rho+\rho_r)(\sigma+\sigma_r)} \tag{31}$$

It is clear, not only from the gains, but also from the time constants that vergence eye movements are different with respect to conjugate eye movements. In normal eye movement, $T_{vergence} >> T_{conjugate}$. This means that responses of conjugate eye movements are far faster than the one of vergence eye movements. In practice, this means that both eyes can together easily follow targets of each eye that are moving with the same velocity and direction, but that it is difficult for the two eyes to follow gazing

targets that have different velocities or directions. In most cases, the gazing targets of each eye that move with the same velocity and direction are in fact the same target. This characteristic is one of the principles of the "same point gazing tendency" of binocular motor systems, i.e. the two eyes cannot easily gaze at two different targets in natural environments. Of course, the "same point gazing tendency" is also related to stereo image processing in the visual cortex.

VI. The Experiments Using a Robot-Eyes System

A. Structure of the Robot-Eyes System

To confirm the proposed binocular motor system model, we constructed a binocular motor control device (robot eyes) with the same system structure as the model shown in Fig. 10 [56].

This robot has 2 degrees of freedom for each "eyeball" and 1 degree of freedom for the neck. DC motors are used as the actuators (Maxson DC motor, 2322-982-52-235-200 for eyeballs, and M99051-A-1 for neck, Swiss made). The image signals from cameras (CCD camera, TOSHIBA IK-CU43) are taken into the computer via an image processing board (MATROX METEOR II). The target's position and velocity relative to the optical line (camera's central line) can be obtained by image processing using the computer. The results of the image processing are transferred in real time through a PIO board to the computer used for robot control.

The rotary angle of each motor can be detected using its own encoder (MTL, MEH-20-2000, Japan). The encoder in the neck motor is substituted for the horizontal semicircular canals. Fig. 11 is the exterior of the robot-eye system.

Fig. 12(a) is the layout of the robot eyes. Fig. 12(b) is the coordinate system of the robot eyes. As shown in Fig. 12(b), the robot-eye system does not use the symmetrical coordinate systems, since most servomotors are not made as pairs. Use of standard motors results in a slightly different sign convention. $O_{C\text{-}l}$ and $O_{C\text{-}r}$ are the origins of both cameras' fixed coordinate systems. $O_{C\text{-}l}$ is defined at the crossing point of the shaft axes of motor 1 and motor 3, xC-l-axis is defined on the center line of the left camera, and $y_{C\text{-}l}$-axis is defined to be parallel with the lateral pixel line of the CCD camera. In this robot-eye system, the $y_{C\text{-}l}$-axis is up on the shaft axis of motor 3. The right eyeball fixed coordinate system $x_{C\text{-}r}$-$y_{C\text{-}r}$-$z_{C\text{-}r}$ is similar to the left one.

The $z_{O\text{-}l}$-axis of the left "orbit" fixed coordinate system ($x_{O\text{-}l}$-$y_{O\text{-}l}$-$z_{O\text{-}l}$) is defined along the shaft axis of motor 1, and the $y_{O\text{-}l}$-axis is defined parallel to the line $O_{C\text{-}l}$-$O_{C\text{-}r}$. The right orbit fixed coordinate system ($x_{O\text{-}r}$-$y_{O\text{-}r}$-$z_{O\text{-}r}$) is similar to the left. The z_H-axis of the head-fixed coordinate system (x_H-y_H-z_H) is defined along the shaft axis
of motor 0 and the plane x_H-y_H passes through $O_{C\text{-}l}$ and $O_{C\text{-}r}$. The x_H-axis is defined parallel to $x_{O\text{-}l}$ and $x_{O\text{-}r}$. O_B is the origin of the base coordinate system (x_B-y_B-z_B). The z_B-axis is defined along the shaft axis of motor 0. In Fig. 12(b), the rotation angles of motor 0, motor 1, motor 2, motor 3 and motor 4 are expressed as θ_0, θ_1, θ_2, θ_3, and θ_4.

Since we consider only horizontal eye movements, the control loops of motors 3 and 4 will not be explained here, i.e. the translation of the head in the direction of the z_H axis and the rotations θ_3 and θ_4 will not be considered. The horizontal coordinate systems of Fig. 12(b) are drawn in Fig. 13. Since the robot-eye system has no degree of freedom for translation, in the real system $x_{hb} = 0$, $y_{hb} = 0$. In the experiments in the case of head translation, $x_{hb}(t)$, $y_{hb}(t)$ and "retinal error" $\varphi_{c\text{-}l}$ and $\varphi_{c\text{-}r}$ (corresponding to $\varphi_{et\text{-}l}$ and - $\varphi_{et\text{-}r}$ in Fig. 4), will be given by computer directly. Comparing Fig. 13 and Fig. 4, the desired values of each "eyeball" (camera center line) are given as the following equations using (10), (11):

$$\varphi_l(t) = -\theta_0(t) + \tan^{-1}\frac{y_t(t) - y_{hb}(t) - r_{hc}\sin(\theta_0(t) + \varphi_{hc})}{x_t(t) - x_{hb}(t) - r_{hc}\cos(\theta_0(t) + \varphi_{hc})} \tag{32}$$

$$\varphi_r(t) = -\theta_0(t) + \tan^{-1}\frac{y_t(t) - y_{hb}(t) - r_{hc}\sin(\theta_0(t) - \varphi_{hc})}{x_t(t) - x_{hb}(t) - r_{hc}\cos(\theta_0(t) - \varphi_{hc})} \quad (33)$$

$\theta_{0,}$ $\theta_{1,}$ and $\theta_{2,}$correspond to φ_{hb}, $\varphi_{eo\text{-}l}$, and $\varphi_{eo\text{-}r}$, while and correspond to $\varphi_{ot\text{-}l}$ and $\varphi_{ot\text{-}r}$, respectively.

B. Image processing for the robot eyes

For this work, we used a white ball as the target of the robot-eye system. Image processing includes: 1) obtaining the gray-level histogram, 2) binalization using the histogram, 3) edge extraction, 4) circle detection using Hough transformations, 5) checking the color of the original image in the circles, 6) labeling the extracted circles, 7) calculating the velocity of the circles, 8) detecting the background movement, 9) detecting the moving object relative to the background. Fig. 14 shown an example of the display of the computer for image processing. The mark + is the position of the target point, as obtained through methods 1)-7) listed above. The mark ○ represents the object that is moving fastest in the visual field. The arrows at each side of the visual fields represent the position of the background. Further discussion of the details of the image processing will be foregone here, as it is not relevant to the main thrust of this work. In the following experiments, only the target.s position and its velocity are used. The processing cycle time is 66-166 ms.

C. The control system for the robot eyes

The control system for the robot-eyes, as shown in Fig. 15, is based on Fig . 9 and (6), (7). $\ddot{\theta}_0(t)$ is the rotational acceleration of the "head" detected by the encoder of motor 0, which corresponds to $\ddot{\varphi}_{v-l}(t)$ and $\ddot{\varphi}_{v-r}(t)$. $\ddot{x}_h(t)$ is the acceleration of the .head. in the x_H direction, which corresponds to $\ddot{x}_{v-l}(t)$ and $\ddot{x}_{v-r}(t)$, and $\ddot{y}_h(t)$ is the acceleration of the .head. in the y_H direction which corresponds to $\ddot{y}_{v-l}(t)$ and $\ddot{y}_{v-r}(t)$. Since the robot-eye system has only one encoder to detect the rotational angle of head $\theta_{0,}$, the pair sensors for detecting head movements as in the human eye system in Fig. 9 cannot be realized, and the translation movements $\ddot{x}_h(t)$ and $\ddot{y}_h(t)$ are given by the computer.

The motor control systems (in the dashed-line boxes) are based on the PID control law, and the parameters of PID control loops are defined by the ultimate sensitivity method. The sampling time is 3ms. As motor control system errors are very small compared to image detection errors and delays, the transfer functions of these systems can be considered to be unity.

From Fig. 15 and (25) the following equation is obtained (see (25)).

$$\begin{bmatrix}\theta_1(s)\\ \theta_2(s)\end{bmatrix} = \\ +\frac{T_{vm}(\rho-\rho_r)}{1+T_{vm}(\rho-\rho_r)(\sigma-\sigma_r)+T_{vm}(1+(\rho-\rho_r)(\eta-\eta_r))s} \\ \times\left(-\frac{\kappa_{hx}T_v}{T_v s+1}\ddot{x}_h(s)+\frac{1}{2}((\sigma-\sigma_r)+(\eta-\eta_r)s)(\varphi_l(s)-\varphi_r(s))\right)\begin{bmatrix}1\\-1\end{bmatrix} \\ +\frac{T_{vm}(\rho+\rho_r)}{1+(\rho+\rho_r)(\sigma+\sigma_r)T_{vm}+(1+(\rho+\rho_r)(\eta+\eta_r))T_{vm}s} \\ \times\left(-\frac{\kappa_{hy}T_v}{T_v s+1}\ddot{y}_h(s)-\frac{\kappa_{h\theta}T_s}{T_s s+1}\ddot{\theta}_0(s)+\frac{1}{2}((\sigma+\sigma_r)+(\eta+\eta_r)s)(\varphi_l(s)+\varphi_r(s))\right)\begin{bmatrix}1\\1\end{bmatrix} \quad (34)$$

If the target is fixed and the head is rotated at the acceleration a, (34) becomes,

$$\begin{bmatrix}\theta_1(s)\\ \theta_2(s)\end{bmatrix} = \frac{T_{vm}(\rho+\rho_r)}{1+(\rho+\rho_r)(\sigma+\sigma_r)T_{vm}+(1+(\rho+\rho_r)(\eta+\eta_r))T_{vm}s} \\ \times\left(-\frac{\kappa_{h\theta}T_s}{T_s s+1}\frac{a}{s}((\sigma+\sigma_r)+(\eta+\eta_r)s)\frac{a}{s^3}\right)\begin{bmatrix}1\\-1\end{bmatrix} \quad (35)$$

Using the initial value theorem,

$$\begin{bmatrix}\ddot{\theta}_1(0)\\ \ddot{\theta}_2(0)\end{bmatrix} = \lim_{s\to\infty}\begin{bmatrix}s^3\theta_1(s)\\ s^3\theta_2(s)\end{bmatrix} = \left(\frac{-\kappa_{h\theta}(\rho+\rho_r)+1}{1+(\rho+\rho_r)(\eta+\eta_r)}-1\right)\begin{bmatrix}a\\-a\end{bmatrix} \quad (36)$$

It is clear that

$$\begin{bmatrix}\ddot{\theta}_1(0)\\ \ddot{\theta}_2(0)\end{bmatrix} = \begin{bmatrix}-a\\ a\end{bmatrix}$$

is the best performance in this case. Therefore,

$$1-\kappa_{h\theta}(\rho+\rho_r)=0 \quad (37)$$

So, in he robot eye control system, the parameters are set according to (29), (37) and tuned by experimental repetition. The one of effective performing sets is $\kappa_{h\theta}$=0.5, ρ = 1.5, ρ_r = 0.5, κ_{hy}=0.2 rad./m, σ = 1, σ_r =0.5, η = 0.5, η_r=0.2, κ_{hy} = 2.0 rad./m.

Physiological experiments suggest that the time constant of the neural integrator is 15-30 s [4], [6], [13], the time constant of the semicircular canal is about 4-6 s [14], [30] and that of the otolith is 0.2-0.3 s [18]. In this work, the time constants are set as , T_{vm}= 25 s, T_s= 6 s, T_v=0.25 s.

In the initial state, the x_H and y_H axis of the head fixed coordinate system of the robot-eye system are set to match the base coordinate system, and the x_E and y_E axis of the eyeball fixed coordinate systems are set to match the orbit fixed coordinate systems, i.e.

$$x_{hb}(0) = 0 \text{ m},\ y_{hb}(0) = 0 \text{ m},\ \dot{x}_h(0) = 0 \text{ m/s},\ \dot{y}_h(0) = 0 \text{ m/s}$$
$$\theta_0(0) = 0 \text{ rad},\ \theta_1(0) = 0 \text{ rad},\ \theta_2(0) = 0 \text{ rad}$$

The target position is set at x_t(0)=1m, y_t(0)=0m. Notice $\dot{x}_h$ and $\dot{y}_h$ are the velocities of

head on the directions of x_h and y_h axes. When $\theta_0(t) \neq 0$, $\dot{x}_{hb}(t) \neq \dot{x}_h(t)$ and $\dot{y}_{hb}(t) \neq \dot{y}_h(t)$.

D. Experiments to Confirm Characteristics of Conjugate and Vergence Eye Movement

1. *The characteristics of same point gazing tendency*

The skillful relation of conjugate and vergence movement of human eyes leads to certain abilities, such as that
both eyes can easily catch the same target point on the central pits of the retinas. In this experiment, we confirm the occurrence of the same point gazing tendency in the robot eyes.

The circumstances of the experiments are shown in Fig. 16. we first fixed the head in place and set a fixed target in front of the head. Then we shown a pendulum swinging from right to left. The weight on the top of the pendulum had the same shape as the first target, and became the second target. The experiment was repeated countless times. Each time, both eyes simultaneously looked at only one target, either the first or the second. One of the experiment results is shown in Fig. 17, which shows t moment that both eyes moved their gaze from the first to the second target.

Fig. 17 shows the desired values φ_l and φ_r, as calculated from the geometry. ${}^1\varphi_l$ and ${}^1\varphi_r$, are the locus of the first target related to each orbit fixed coordinate system. ${}^2\varphi_l$ and ${}^2\varphi_r$ are the locus of the second target, and $\varphi_{C\_l}(t)$ and $\varphi_{C\_r}(t)$ are the .retinal errors. (errors detected by image processing). t_1 shown in Fig. 17 marks the instant that the second target was shown to the robot eyes. t_2 marks the instant the left eye recognized the second target, and from t_3 to t_5, the left eye lost its target. t_4 and t_5 are the instants that the right eye and the left eye recognized the second target. Fig. 17 shows that when the left eye recognizes the second target at t_2, the left eyeball (θ_1) begins to leave the first target and pulls the right eyeball (θ_2) to leave the first target as well. This causes the right eye to recognize the second target (the object nearest the central pit is processed at the highest priority). There are cases when the right eye does not recognize the second target and pulls the left eyeball to recognize the first target again. Here the concept of one eye .pulling. the other is a result of the system characteristics of slow vergence control and fast conjugate control.

2. *The behavior when one eye is prevented from viewing the target*

When an eye is shut or the target is blocked with an obstacle, the obstructed eye moves with the other eyeball. This characteristic lets the eye catch up to the target quickly when the obstacle is removed. The following experiment confirms the occurrence of conjugate eye movement:

we fixed the head and set a target on the top of a pendulum, then swung it from right to left in front of the head. The circumstances of the experiments are shown in Fig. 18. One set of experimental results is shown in Fig. 19. In the time between t_1 and t_2, the right eye was obstructed using a mask as shown in Fig. 18(a). Fig. 19 shows that even though the right eye cannot follow the target accurately while it is blocked, it tracks the target very smoothly when the mask is taken off.

3. *Characteristics of vergence eye movement*

If a binocular motor control system had only conjugate eye movement capabilities, the binocular nature of the system would not have any significance because it would mean the two eyeballs were fixed to each other, or that the eyeballs were driven by the same signals. Vergence eye movement is needed to catch a target at the central pits of both eyes when the target is approaching or receding from the eyes, as shown in Fig. 20. To observe the characteristics of vergence eye movement of the robot eyes, the step response was obtained via the following experiment.

The head was fixed and the initial positions of each eyeball were set to parallel with the midline, namely,

$$x_{hb}(t)=0 \text{ m}, \; y_{hb}(t)=0 \text{ m}, \quad \theta_0(t)=0 \text{ rad}, \; \theta_1(0)=0 \text{ rad}, \; \theta_2(0)=0 \text{ rad},$$

A target was set at the position:

$$r_{ht}=0.2 \text{ m}, \; \varphi_{ht}=-5 \text{ deg}=-0.087 \text{ rad}.$$

From (30) and (31), the desired values of each eyeball are:

$$\varphi_l(t) = \tan^{-1} \frac{r_{ht}\sin\varphi_{ht} - r_{he}\sin\varphi_{he}}{r_{ht}\cos\varphi_{ht} - r_{he}\cos\varphi_{he}} \tag{38}$$

$$\varphi_r(t) = \tan^{-1} \frac{r_{ht}\sin\varphi_{ht} + r_{he}\sin\varphi_{he}}{r_{ht}\cos\varphi_{ht} - r_{he}\cos\varphi_{he}} \tag{39}$$

The robot eyes were designed with:

$$r_{he}=0.09 \text{ m}, \; \varphi_{he}=22.88 \text{ deg}=0.400 \text{ rad}.$$

So, from equations (38) and (39),

$$\varphi_l = -24.3 \text{ deg} = -0.424 \text{ rad}, \quad \varphi_r = 8.6 \text{ deg} = 0.150 \text{ rad}$$

are obtained. Fig. 21 shows the controlled errors $(\varphi_{l-r}(t) \text{ and } \varphi_{l-r}(t))$ become 0, and the eyeballs. positions $(\theta_1(t), \theta_2(t))$ close to the desired values (φ_l, φ_r). Fig. 21 also shows that the settling times of vergence eye movement are much slower compared to those of conjugate eye movement.

From (25) or (34) if $\rho=\rho_r \text{ or } \sigma=\sigma_r, \; \eta=\eta_r,$ the vergence eye movement will disappear. The results of the same experiment with $\rho=\rho_r$ are shown in Fig. 22. Fig. 22 shows $\theta_1(t) \text{ and } \theta_2(t)$ moving together completely, i.e. there is no vergence movement.

E. The Experiments of VOR for Head Rotations

(a) Fix the target and rotate the head

An experiment was made by fixing the target at $x_t(0)$=1m, $y_t(0)$=0m. and rotating the head according to the following equation:

$$\theta_0(t) = \frac{\pi}{6}\sin(\frac{\pi}{3}t) \tag{40}$$

In this case, it is chosen:

$x_h(t)=y_h(t)=0$m

Fig. 23(a) shows the result of the experiment. Since the left eye has the same characteristics as the right one, we shown only the right eye's rotation $\theta_2(t)$ in Fig. 23. The desired value φ_r in the figure is obtained from equation (33).

(b) Cut the VOR control loop

The same experiment as in (a) was done, but with $\kappa_{h\theta}=0.$ The rotation of the right eyeball is shown in Fig. 23 (b). Since there are no vestibular reflex control loops in the control system with this parameter set, this experiment is similar to fixing the head and rotating the target around the head according to

$$\varphi_{hd}(t) = -\frac{\pi}{6}\sin(\frac{\pi}{3}t) \tag{41}$$

(c) Rotate the head in darkness

In this case the image feedback signals are regarded as 0. The head was rotated according to equation (40), the experimental result is shown in Fig. 23 (c).

It is clear from Fig. 23 that the target tracking in case (a) performed better than in the other cases. In contrast, an obvious delay with respect to the target is shown for the pursuit movement if the image feedback works alone in the experiment (b). On the other hand, since VOR is only related to head movements, the pursuit precision will be never guaranteed when VOR works alone, as shown in experiment (c).

F. The Experiments of Head Translations

Since the robot-eye system has no degree of freedom for translational motion, in the experi nts described as follows, the translation signals of the head $\ddot{x}_h(t)$, $\ddot{y}_h(t)$, and the image signals from the CCD cameras $\varphi_{C\text{-}l}(t)$, $\varphi_{C\text{-}r}(t)$ were given by the computers directly. The sampling time of $\varphi_{C\text{-}l}(t)$ and $\varphi_{C\text{-}r}(t)$ was set to 100ms.

1. *Characteristics of conjugate for head translations*

(a) Fix the target and translate the head in y_H direction

In this case, it is chosen

$$y_t(t)=0\,\text{m},\quad x_t(t)=1\,\text{m},\quad \theta_0(t)=0\,\text{rad}.$$

and consider that the head translates in the y_H direction according to the following equation:

$$x_{hb}(t)=0\,\text{m},\quad y_{hb}(t)=0.5\sin(\pi t/3)\,\text{m} \tag{42}$$

So, the input signal for VOR is:

$$\ddot{x}_h(t)=0,\quad \ddot{y}_h(t)=\pi^2/18\sin(\pi t/3),\quad \ddot{\theta}_0(t)=0 \tag{43}$$

From equations (32) and (33),

$$\varphi_l(t)=\tan^{-1}\frac{-0.5\sin(\pi t/3)-r_{hc}\sin\varphi_{hc}}{1-r_{hc}\cos\varphi_{hc}} \tag{44}$$

$$\varphi_r(t)=\tan^{-1}\frac{-0.5\sin(\pi t/3)+r_{hc}\sin\varphi_{hc}}{1-r_{hc}\cos\varphi_{hc}} \tag{45}$$

The "retinal error" signals are calculated as

$$\varphi_{C-l}(t) = \varphi_l(t) - \theta_1(t) \quad (46)$$

$$\varphi_{C-r}(t) = -\varphi_r(t) - \theta_2(t) \quad (47)$$

Fig. 24(a) shows the results of the experiment. Here, only the right eye's rotation $\theta_2(t)$ is shown.

(b) Fix the head and move the target in the y_B direction

In this case, it is chosen

$x_{hb}(t)=0\,\text{m},\quad y_{hb}(t)=0\,\text{m},\quad \theta_0(t)=0\,\text{rad}$

The target position was set according to the following equation:

$$x_t(t) = 1\ \text{m},\quad y_t(t) = -0.5\sin(\pi t/3) \quad (48)$$

From equations (32) and (33),

$$\varphi_l(t) = \tan^{-1}\frac{-0.5\sin(\pi/3) - r_{bc}\sin\varphi_{bc}}{1 - r_{bc}\cos\varphi_{bc}} \quad (49)$$

$$\varphi_r(t) = \tan^{-1}\frac{-0.5\sin(\pi/3) + r_{bc}\sin\varphi_{bc}}{1 - r_{bc}\cos\varphi_{bc}} \quad (50)$$

Fig. 24 (b) shows the results of the experiment.

(c) Translate the head in y_H direction in darkness

The same experiments as in (a) were performed, but in darkness. In this case the .retinal error. signals $\varphi_{C-l}(t)$ and $\varphi_{C-r}(t)$ were set to 0. The experiment results are shown in Fig. 24 (c). Since the time constants of the otoliths are too short (0.25 s), and the best gains of the VOR-T pathways are related to the distance to the target, the response of VOR working alone is far inferior to the desired behavior. However, the experiments described below show that when the head moves at high frequencies, the VOR-T response becomes better.

For example the head was moved as described by the following equation:

$y_h(t) = 0.5\sin(2\pi t)$

The others conditions were identical to those used for the experiments whose results are presented in Fig. 24. The experiment results are shown in Fig. 25, and Fig. 25 shown that similar to VOR-R, VOR-T also has better response characteristics in the high frequency domain [55], but that the "cut-off frequency" is far higher for VOR-T than for VOR-R.

2. *The characteristics of vergence for translate motions*

(a) Fix the target and move the head in the x_H direction

In this case, it is chosen:

$x_t(t) = 1\,\text{m},\quad y_t(t) = 0\,\text{m},\quad \theta_0(t) = 0\,\text{rad}$

The head is assumed to move in the x_H direction according to the following equation:

$$x_{hb}(t) = 0.5\sin(\pi/6),\quad y_{hb}(t) = 0\,\text{m} \quad (51)$$

So, the input signal for VOR is

$$\ddot{x}_h(t) = \pi^2/72\cos(\pi t/6) \quad (52)$$

From (32) and (33), the desired values of the robot eyes are:

$$\varphi_l(t) = -\tan^{-1}\frac{r_{bc}\sin\varphi_{bc}}{1 - 0.5\sin(\pi/6) - r_{bc}\cos\varphi_{bc}} \quad (53)$$

$$\varphi_r(t) = \tan^{-1}\frac{r_{hc}\sin\varphi_{hc}}{1-0.5\sin(\pi/6)-r_{hc}\cos\varphi_{hc}} \tag{54}$$

Fig. 26(a) shows the experimental results.

(b) Fix the head and move the target in the x_B direction

In this case, it is chosen:

$$x_{hh}(t) = 0 \text{ m}, \quad y_{hh}(t) = 0 \text{ m}, \quad \theta_h(t) = 0 \text{ rad}.$$

The target position was set according to the next equation.

$$x_t(t) = 1-0.5\sin(\pi t/6), \quad y_t(t) = 0 \text{ m} \tag{55}$$

The desired values of the robot-eyes are the same as (53) and (54). Fig. 26 (b) shows the results of the experiment.

(c) Translate the head in the x_H direction in darkness

In this case the retinal errors signals were set to:

$$\varphi_{C\text{-}l}(t)=0, \ \varphi_{C\text{-}r}(t)=0.$$

The other conditions were the same as in (a). The experimental results are shown in Fig. 26 (c).

Similar to conjugate VOR, the phase shift of vergence VOR becomes smaller when the frequency of head movement is higher. Furthermore, the optimal neural pathway gain for vergence VOR is related to the distance from the eyes to the target.

VII RESULTS AND DISCUSSIONS

An eyeball is only able to rotate, not translate, in its socket. However, it has to adjust not only for the head and target rotations around its center of rotation, but also for their translations. As a result, apparently similar eye movements can be caused by quite different signals detected by semicircular canals, otoliths or retinas. Therefore, analysis of the phenomena of the eyeball rotational responses to the numerous input signals of the ocular motor system becomes very difficult. In this paper we have reclassified the different types of eye movements according to the kinds of input signals to the ocular motor control system that produce them.

Except saccade movements, which have not been discussed in this paper, the definitions of horizontal binocular eye movements are given by equations (23) and (24) and are as follows:

a. Conjugate VOR is the eye movement response that comes as a result of differences between the signals from the right and left vestibular organs. In the normal state the signals from the horizontal semicircular canals and otoliths relate to head rotations and lateral head translations [see (25)].

b. Vergence VOR is eye movement that responds to the sums of the signals from the right and left vestibular organs. In the normal state the signals come from the otoliths and relate to cross directional head translations [see (25)].

c. Conjugate smooth pursuit is eye movement that responds to the difference between the

right and left retinal error signals.
d. Vergence smooth pursuit is the eye movement response that follows the sum of the right and left retinal error signals.
e. Conjugate optokinetic response is the eye movement response that is caused by the difference between the signals measuring the right and left retinal slip velocity.
f. Vergence optokinetic response is the eye movement response that follows the sum of the signals measuring the right and left retinal slip velocity.
The transfer functions of the binocular model show that the conjugate and vergence eye movements have different dynamic characteristics, even though they have the same control system. Only when all of the crossing pathways are broken (i.e. $\rho_r = 0$, $\sigma_r = 0$, $\eta_r = 0$, $\kappa_{xr} = 0$, $\kappa_{yr} = 0$, $\kappa_{\phi r} = 0$ see Fig. 9), do conjugate and vergence have the same dynamic characteristics; that means, however, that both eyes have independent control systems. As is the case for VOR and smooth pursuit, in my opinion that vergence saccade is also far slower than the conjugate saccadic response.
Although physiological experiments have found an area in the cortex that can cause ve ence movements [15], we still believe that the basic neural network shown in Fig. 1 has the ability to cause vergence movements.
Since vergence smooth pursuits always move slowly compared to conjugate smooth pursuits, the neural signals would be very weak to measure. Other, faster vergence movements related to signals from such as convergence and divergence burst cells [27], [28] can be considered as vergence saccade, which was not discussed in this paper.
The transfer function of VOR for translations shows that the centrifugal forces on the macula of utricles may cause vergence VOR, and that appropriate transmission gains on the signals from the utricles on both sides to the vestibular nucleus can cancel the influence of centrifugal forces on eye movements. This means if there are lesions in the binocular motor system, which disturb the balance of the signal transmission gains, the centrifugal accelerations will cause unnecessary eye movements [54].
The characteristic of "same point gazing tendency" was realized using the proposed robot-eye system. This characteristic allows the two eyes to take in a pair of symmetrical images with the same target point in the central pits, and In my opinion this characteristic is one of the basic conditions for creating a stereovision space in the visual cortex using images from both retinas.

In the near future, more complete oculomotor system models should be built upon the framework laid out in the model proposed here. Likely beneficial engineering application of this work includes assistance to the development of artificial eye systems, which are one of the most important "organs" in modern robotics. Furthermore, this work may aid the field of medicine by helping to pioneer some new areas, such as the location diacritics of neuro-ophthalmology using eye movement patterns that correspond to head or target movement patterns, based on oculomotor system models [54].

REFERENCES

[1] Baker, R., C. Evinger, R. A. McCrea, "Some thoughts about the three neurons in the

vestibular ocular reflex," Vestibular and oculomotor physiology, B. Cohen, Ed., NY Academy of Sciences, Part IV, pp.
171-188, 1981.
[2] Barnes, G. R., "Vestibular control of oculomotor and postural mechanisms," *Clin. Phys. Physiol. Meas.*,
vol. 1, pp. 3-40, 1980.
[3] Buizza, A., A. Leger, J. Droulez, A. Berthoz, and R. Schmid, "Influence of otolithic stimulation by horizontal linear acceleration on optokinetic nystagmus and visual motion perception." Exp. Brain Res. Vol.39, pp.165-176, 1980.
[4] Cannon, S.C., D.A. Robinson, "Loss of the neural integrator of the oculomotor system from brain stem lesions in monkey," *J. Neurophysiol.* 57-5, 1383-1409, 1987.
[5] Cannon, SC., D.A. Robinson, "An improved neural-network model for the neural integrator of the oculomotor system: more realistic neuron behavior." Biol. Cybern. Vol.53, No.2, pp.93-108, 1985.
[6] Chun, K. S., D.A. Robinson, "A model of quick phase generation in the vestibuloocular reflex." Biological Cybernetics. Vol.28, No.4, pp.209-21, 1978.
[7] Cova, A C, H.L. Galiana, "A bilateral model of vergence and the vestibulo-ocular reflex." Exp Brain Res, Vol.107, pp.435 - 452, 1996.
[8] Cova, A.C., H.L. Galiana, "Providing Distinct Vergence and Version Dynamics in a Bilateral Oculomotor Network." Vision Res. Vol.35, No.23/24, pp. 3359 - 3371, 1995.
[9] Erkelens, C.J, R.M. Steinman, and H, Collewijn, "Ocular vergence under natural conditions. II. Gaze-shifts between real target differing in distance and direction." Proc. R. Soc. Lond. B Biol. Sci. 236: pp.441-465, 1989.
[10] Fernandez C., J.M. Goldberg, W.K.Abend, "Response to static tilts of peripheral neurons innervating otolith organs of the squirrel monkey,", J Neurophysiol., 35(6), 978-87, 1972.
[11] Fernandez C., J.M. Goldberg,“ Physiology of peripheral neurons innervating otolith organs of the squirrel monkey. III. Response dynamics.," J Neurophysiol., 39, 996-1008, 1976.
[12] Fuchs A.F., J. Kimm, "Unit activity in vestibular nucleus of the alert monkey during horizontal angular acceleration and eye movement," J. Neurophysiol., vol. 38, pp.1140-1161, 1975 . 35
[13] Galiana H.L., J.S. Outerbridge,"A bilateral model for central neural pathways in the vestibulo-ocular reflex,". J. Neurophysiology, vol. 51, pp. 210-241, 1984.
[14] Galiana H.L.: "A Nystagmus Strategy to Linearize the Vestibulo - Ocular Reflex." IEEE Trans Biomed Eng, Vol.38, No.6, pp.532 - 543, 1991.
[15] Gamlin, P. D., Kyunghee Yoon, "An area for vergence eye movement in primate frontal cortex.", Nature, Vol.407, 26, pp.1003-1007, 2000.
[16] Gary, D. P., D.L. Tomko, "Eye movement responses to linear head motion in the squirrel monkey. II. Visual-vestibular interactions and kinematic considerations." *J. Neurphysiol.* **65**, pp.1183-1196, 1991.
[17] Goldberg, J. M., C. Fernandez, "Physiology of peripheral neurons innervating semicircular canals of the squirrel monkey. I Resting discharge and response to constant

angular accelerations," J. Neurophysiol., vol. 34, pp.635-660, 1971.
[18] Green, A.M., Galiana H.L., "Hypothesis for shared central processing of canal and otolith signals." J Neurophysiol. Vol.80, No.4, pp.2222-2228, 1998.
[19] Hall, Z.W., "An Introduction to Molecular Neurobiology,. New York: Sinauer Associates, 1992.
[20] Israeel, I., A. Berthoz, "Contribution of the otoliths to the calculation of linear displacement," J. Neuroph., Vol.62, No.1, pp. 247-263, 1989.
[21] Jan, L. Y., Y. N. Jan, "Peptidergic Transmission in Sympathetic Ganglia of the Frog." J. Physiol., Vol.327, pp. 219-246. 1982.
[22] Kelle,r E.L., D.A. Robinson, .Abducens unit behavior in the monkey during vergence movements," Vision Research. 12(3): 369-82, 1972.
[23] Komatsuzaki, A, Y. Shinoda, T. Maruo: "Neurology of Oculomotor System", Igaku-Shoin Ltd. Tokyo, 1985.
[24] Malcolm, B. C.: Core text of Neuroanatomy, The Williams & Wilkins / Waverly, Inc., USA, 1991.
[25] Masuda, K, etc: Current Encyclopedia of Ophthalmology (7), Nakayama-Shoten Co., Ltd. Japan, pp.385-528. 1995.
[26] Maxwell, J.S, W.M. King, "Dynamics and efficacy of saccade-facilitated vergence eye movements in monkeys." J Neurophysiol. Vol.68-4, 1248-60, 1992.
[27] Mays, L. E., "Neural Control of Vergence Eye Movements: Convergence and Divergence Neurons in Midbrain." Journal of Neurophysiology, Vol. 51, No. 5, pp.1091-1108, 1984.
[28] Mays, L.E., J.D. Porter, D.R. Gamlin, C.A. Tello, "Neural Control of Vergence Eye Movements: Neurons Encoding Vergence Velocity." Journal of Neurophysiology, Vol. 56, No. 4, pp.1007-1021, 1986.
[29] Mettens, P., E. Godaux, G. Cheron, H.L. Galiana, "Effect of Muscimol Microinjections Into the Prepositus Hypoglossi and the Medial Vestibular Nuclei on Cat Eye Movements," Journal of Neurophysiology, Vol. 72, No.2, pp.785-802, 1994.
[30] Melvill, J., G., J. H. Milsum: "Frequency-response analysis of central vestibular unit activity resulting from rotational stimulation of the semi-circular canals." J. Physiol. (Lond.) Vol.219, 191-215, 1971.
[31] Miles, F.A, "Adaptive regulation in the vergence and accommodation control systems." Reviews of Oculomotor Research. Vol.1, pp.81-94, 1985.
[32] Miller, J.M. Robinson DA., "A model of the mechanics of binocular alignment." Computers & Biomedical Research. Vol.17, No.5, 436-70, 1984.
[33] Paige, G.D., D.L. Tomko, "Eye movement responses to linear head motion in the squirrel monkey. II. Visual-vestibular interactions and kinematic considerations." Journal of Neurophysiol. Vol. 65, pp.1183- 1196, 1991.
[34] Pellionisz, A. "Tensorial aspects of multidimensional approach to the vestibulo-oculomotor reflex and gaze." Reviews of Oculomotor Research. 1: pp.282-296, 1985.
[35] Raphan, T., S. Wearne, B. Cohen, "Modeling the organization of the linear and angular vestibulo-ocular reflexes. " Ann. NY Acad. Sci. Vol.781, pp.348-363, 1996.
[36] Robinson, D.A., "The mechanics of human smooth pursuit eye movement." J. physiol. Vol.39, No.5, pp.569-591, 1965.

[37] Robinson, D.A., "Linear addition of optokinetic and vestibular signals in the vestibular nuclues," Exp. Brain Res., Vol.30, pp.447-450, 1977.
[38] Robinson, D.A., The system approach to the oculomotor system. Vision Res. Vol.26, No.1, pp.91-99, 1986.
[39] Robinson, D.A., "The coordinates of neurons in the vestibulo-ocular reflex. Reviews of Oculomotor Research." 1: pp.297-311, 1985.
[40] Robinson, D.A., "The use of matrices in analyzing the three-dimensional behavior of the vestibulo-ocular reflex." Biological Cybernetics. Vol.46, No.1:53-66, 1982.
[41] Robinson, D.A., "The use of control systems analysis in the neurophysiology of eye movements. Annu" Rev. Neurosci. Vol. 4, pp.463-503, 1981.
[42] Rumelhart, D. E., G.E. Hinton, R.J. Williams, Learning Internal Representations by Back-Propagation Errors, NATURE, Vol.323, 533-536, Oct. (1986).
[43] Semmlow, J.L., T. Tinor, "Accommodative convergence response to off-foveal retinal images," Source Journal of the Optical Society of America. Vol.68(11), pp.1497-1501, 1978.
[44] Shinoda, Y., K. Yoshida, "Dynamic characteristics of responses to horizontal head angular acceleration in vestibuloocular pathway in the cat," J. Neurophysiol. Vol. 37, No.4, pp.653-673, 1974.
[45] Skavenski, A.A., D.A. Robinson, "Role of abducens neurons in vestibulo-ocular reflex," J. Neurophysiol., vol.36, pp. 724-738, 1973.
[46] Smith, H.L., H.L. Galiana, " The role of structural symmetry in linearizing ocular reflexes," Biol. Cybernetics, 1991.
[47] Spoendlin, H.H., "Ultrastructure of the vestibular sense organ,. in .The vestibular system and its diseases.: transactions of the International Vestibular Symposium of the Graduate School of Medicine of the University of Pennsylvania / Edited by Robert J. Wolfson, 1966.
[48] Simpson, J.I, Graf W., "Eye-muscle geometry and compensatory eye movements in lateral-eyed and frontal-eyed animals. Ann N Y Acad Sci. Vol. 374:20-30. 1981.
[49] Simpson, JI, Graf W., "The selection of reference frames by nature and its investigators." Reviews of Oculomotor Research. 1: pp.3-16, 1985.
[50] Telford, L., S.H. Seidman, G.D. Paige, "Dynamics of squirrel monkey linear vestibularoocular reflex and interactions with fixation distance." Journal of Neurophysiol, Vol. 78, pp.1775-1790, 1997.
[51] Uchino, Y., H. Sasaki, H. Sato, M. Imagawa, H. Suwa, and N. Isu, "Utriculoocular Reflex Arc of the Cat." J. Neurophysiol. Vol.76, No. 3, pp. 1896-1903.
[52] Wyatt, H. J., J. Pola, "smooth eye movements with step-ramp stimuli: The influence of attention and stimulus extent," Vision Res., Vol. 27, No. 9, pp. 1565-1580, 1987.
[53] Zee, D.S., E.J. Fitzgibbon, L.M. Optican, "Saccade-Vergence Interaction in Humans," Journal of Neurophysiology, Vol.68, No.5, pp.1624-1641, 1992.
[54] Zhang, X., H. Wakamatsu, A mathematical model for binocular vestibular-ocular reflex and its application on topographic diagnosis. Japanese Journal of Applied Physiology, Vol.**29, No.**2, pp.123-131, 1999.
[55] Zhang, X., H. Wakamatsu, .An Unified Adaptive Oculomotor Control Model,. Int. J.

Adapt. Control Signal Process，Vol.15, No.7, pp.697-713, 2001.
[56] Zhang, X., H. Wakamatsu, .Mathematical model for binocular movements mechanism and construction of eye axes control system,. *Journal of the Robotics Society of Japan* (*JRSJ*), Vol.20, No.1, 89-97, 2002.

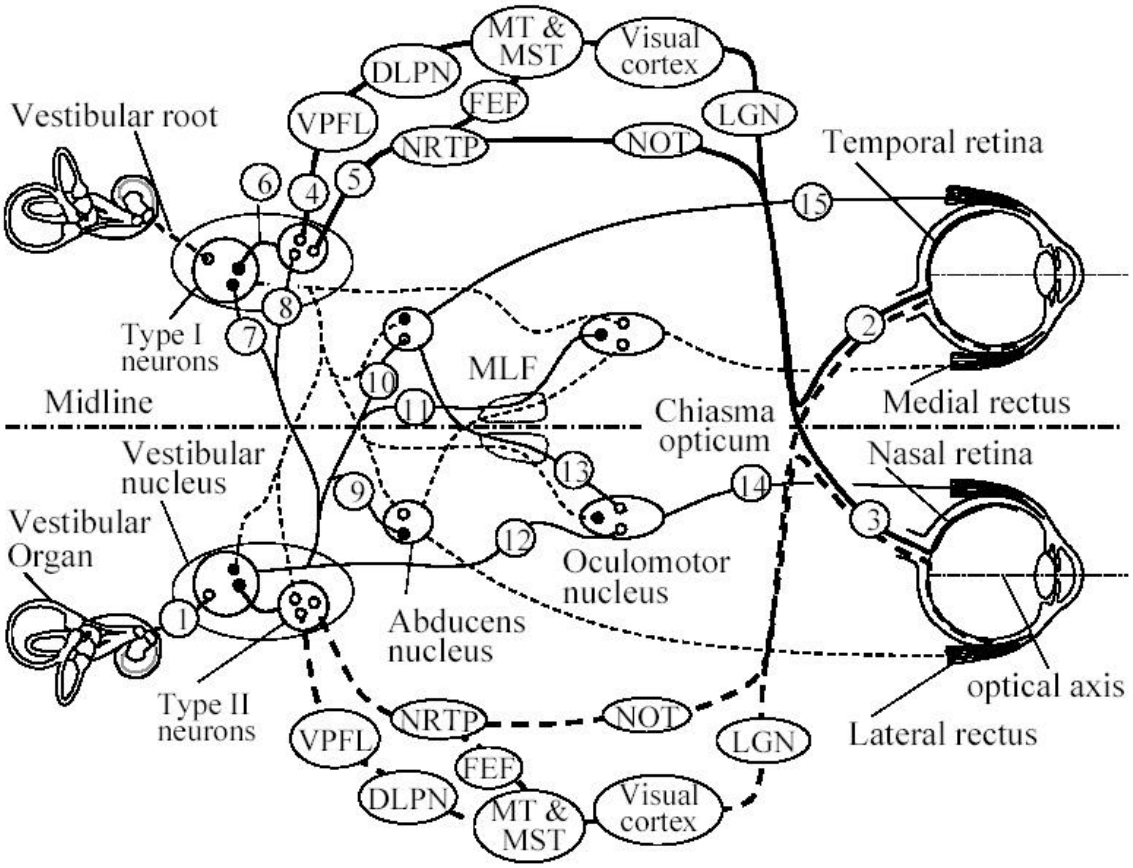

MT: Middle temporal area, MST: Medial superior temporal area, LGN: Lateral geniculate nucleus, NOT: Nucleus of the optic tract, NRTP: Nucleus reticularis tegmenti pontis, DLPN: Dorsolateral pontine nucleus, VPFL: Ventral paraflocculus, FEF: Frontal eye field, MLF: Medial longitudinal fasciculus.

Fig. 1 Neural pathways of horizontal binocular motor system

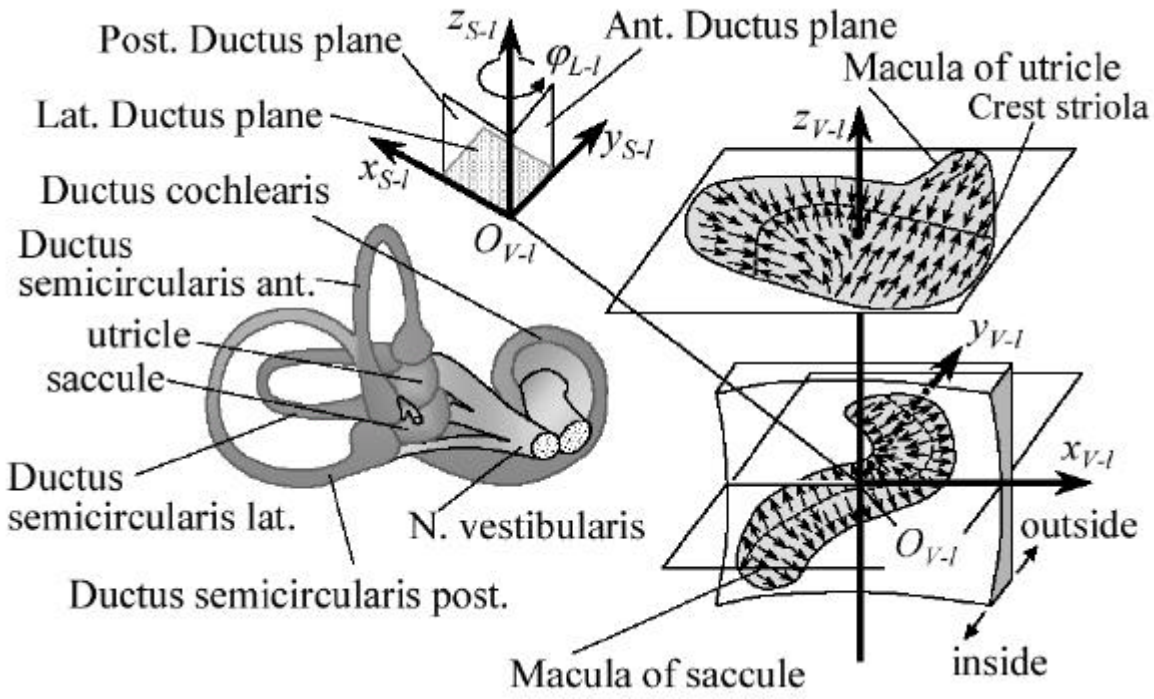

(a) Left side

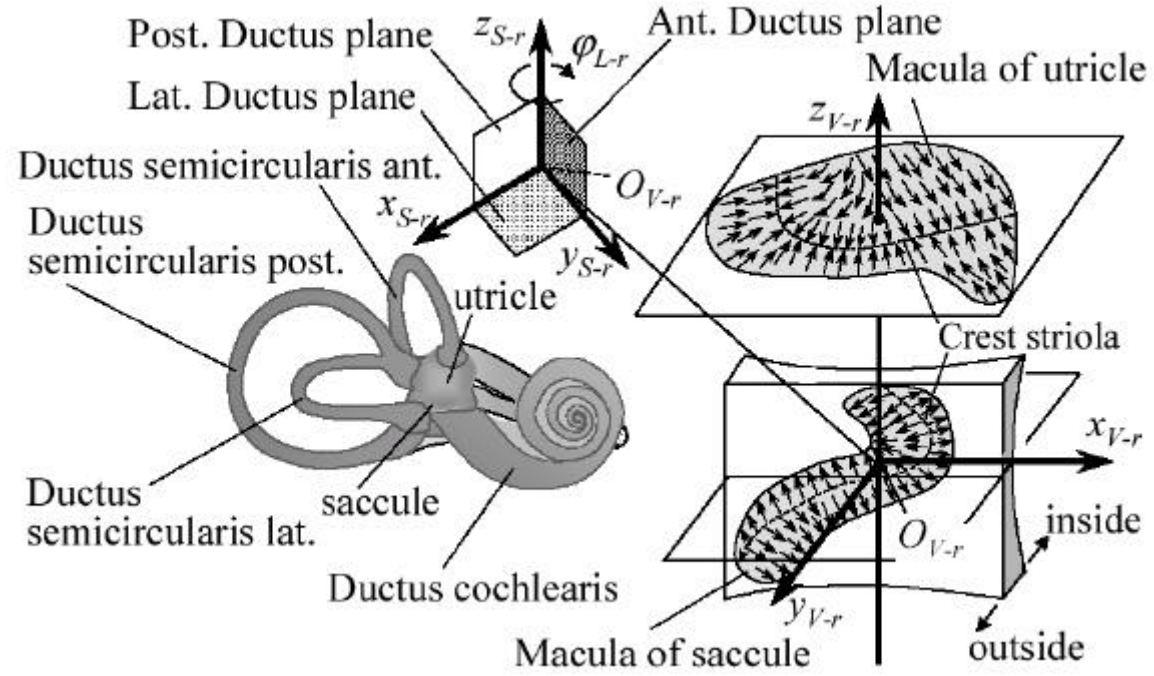

(b) Right side

Fig. 2 The coordinate systems of a vestibular organ

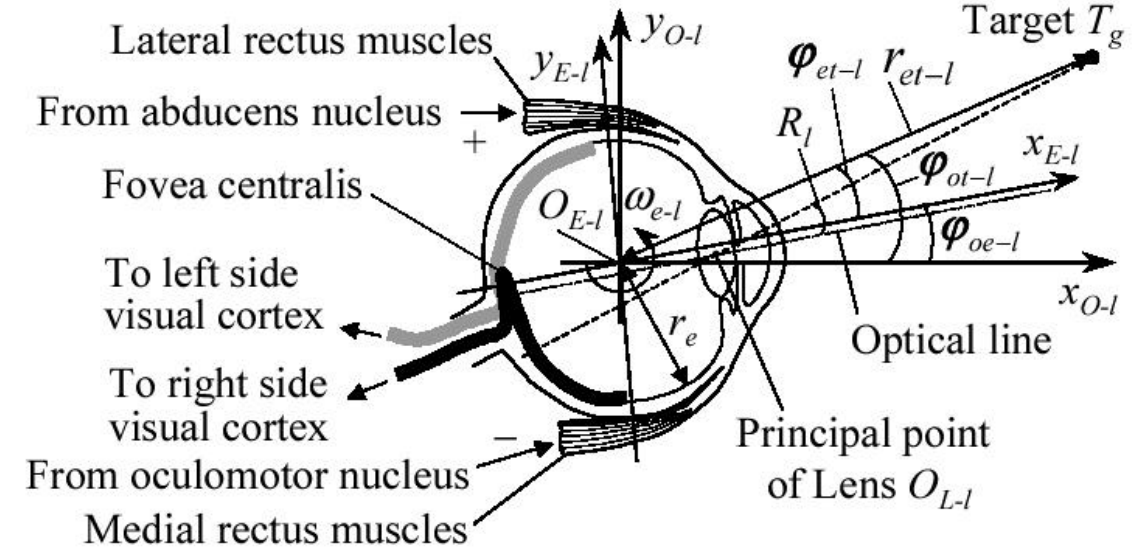

(a) Left eyeball

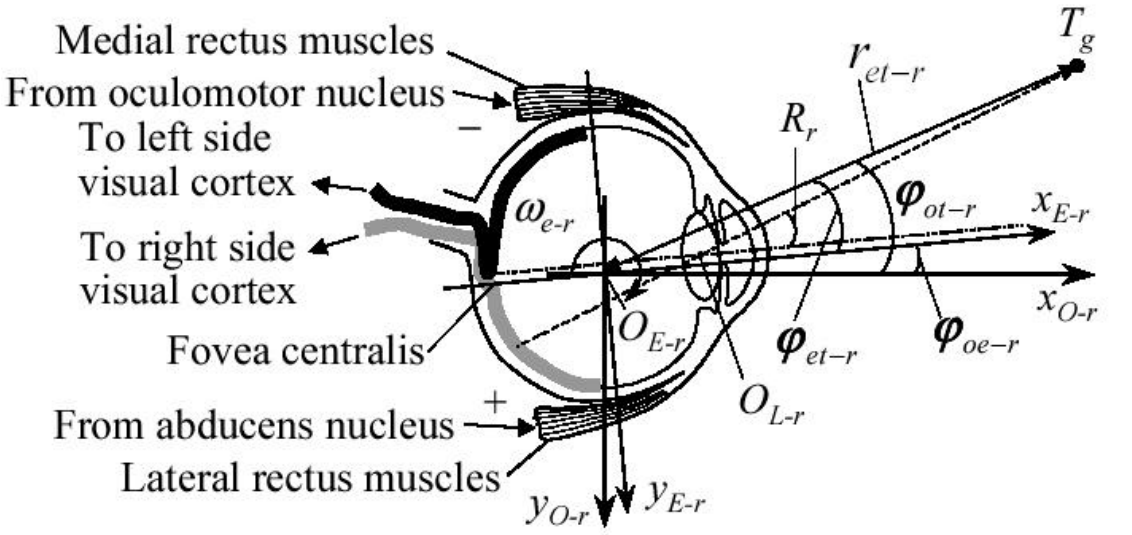

(b) Right eyeball

Fig. 3 Coordinates for eyeballs

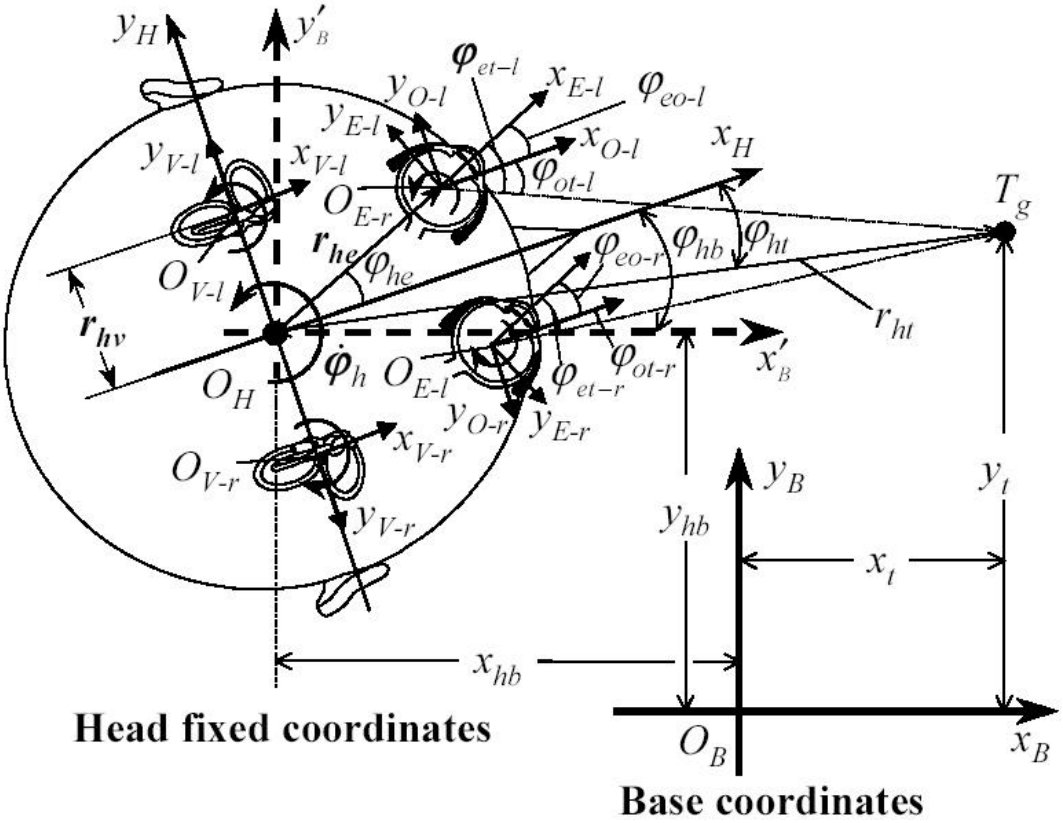

Fig. 4 The coordinate system for head and target

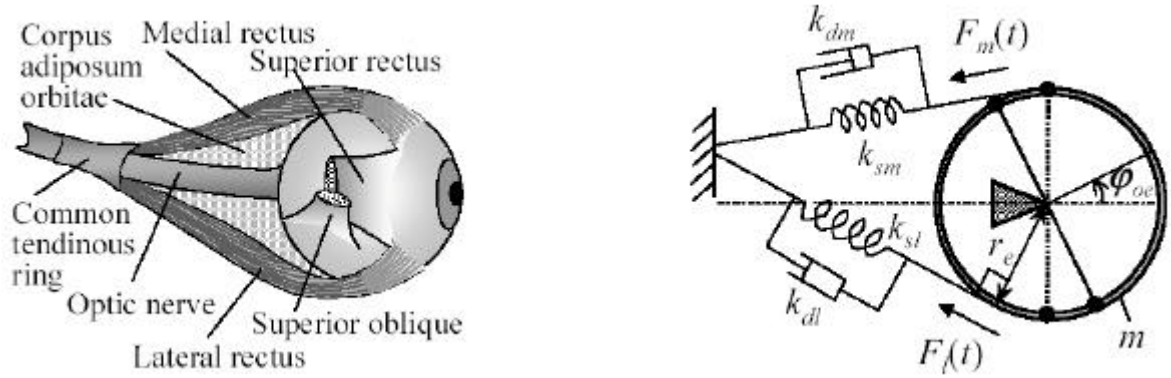

(a) The anatomical structure of right eyeball (b) Viscoelasticity model

Fig. 5 The viscoelastic model of eye plant based on the anatomical structure

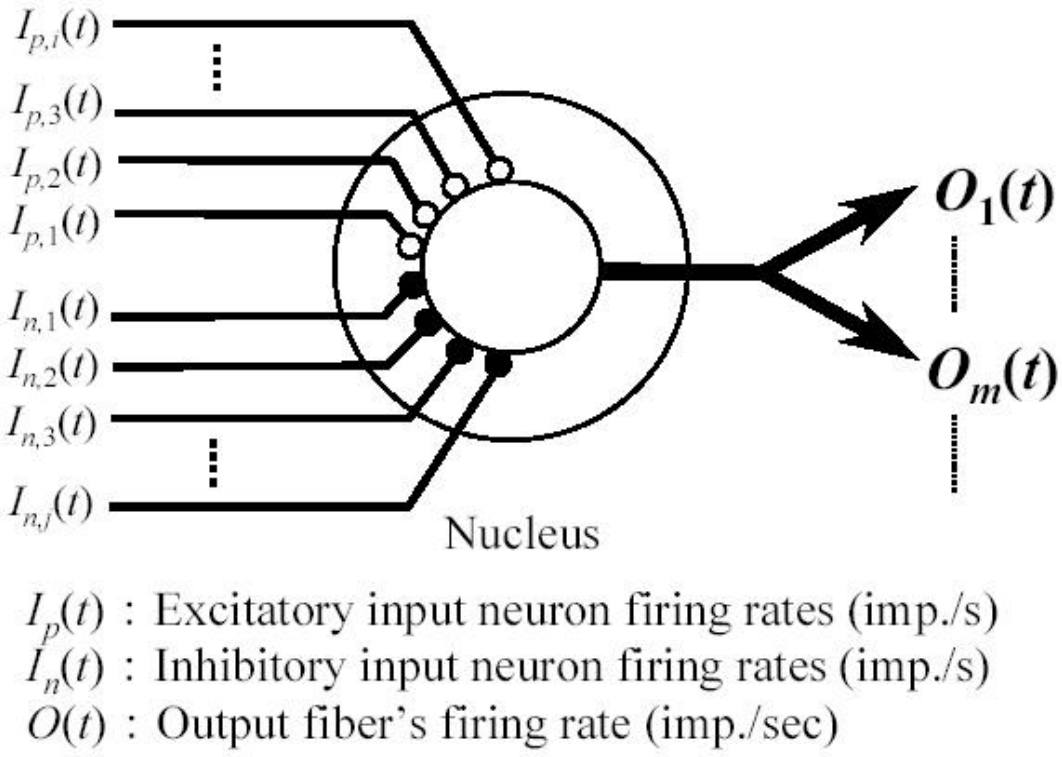

Fig. 6 An imaginary nucleus

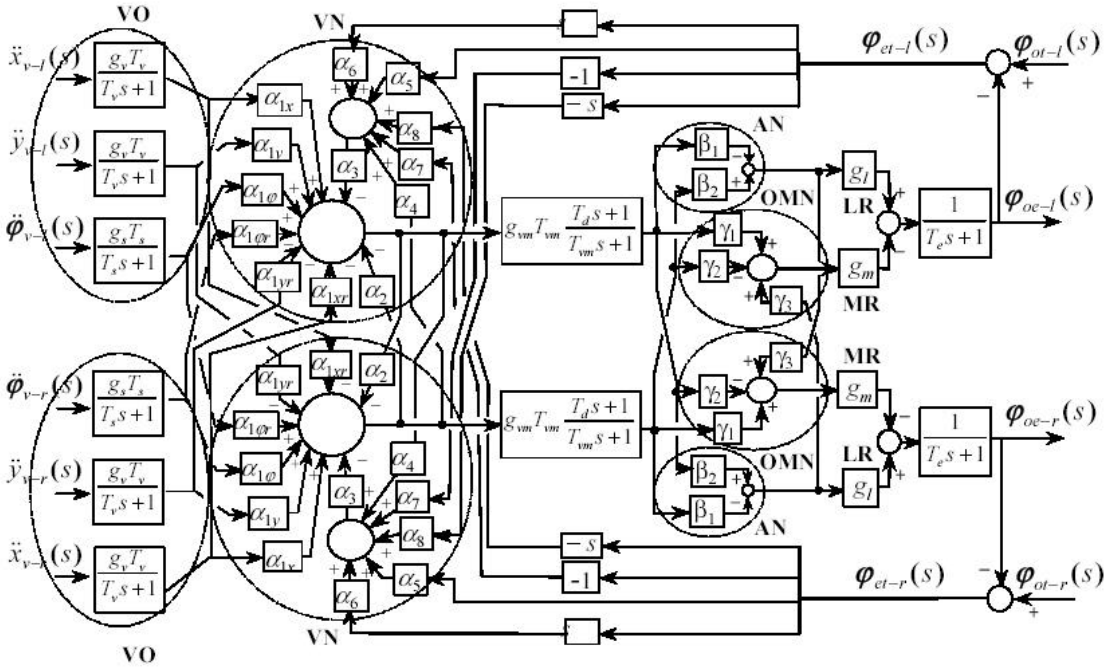

VO: vestibular organ, VN: vestibular nucleus, AN: abducens nucleus,

OMN: oculomotor nucleus, MR: medial rectus, LR: lateral rectus.

Fig. 7 Block diagram of oculomotor system faithful to the physiological structure shown in Fig. 1

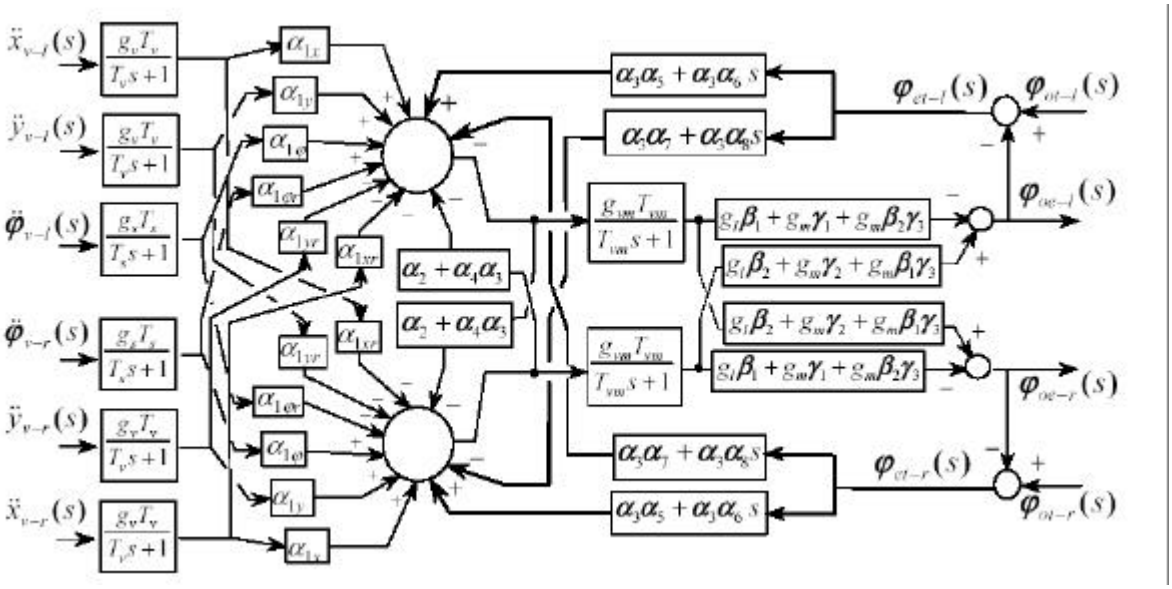

Fig. 8 Block diagram system through rearranging the basic system in Fig. 7

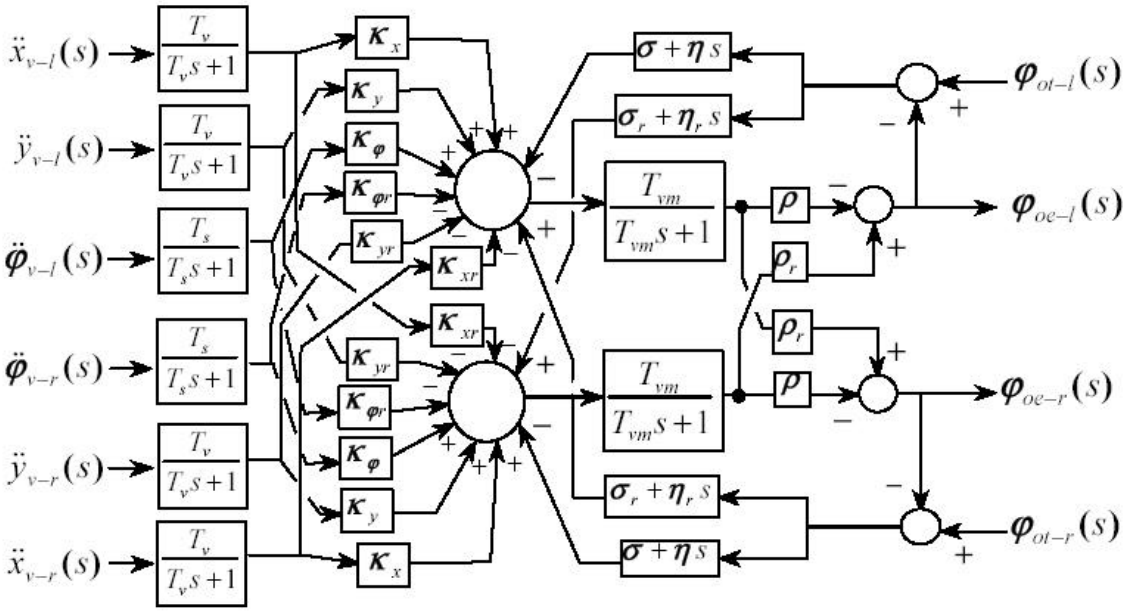

Fig. 9 Simplified binocular motor system model

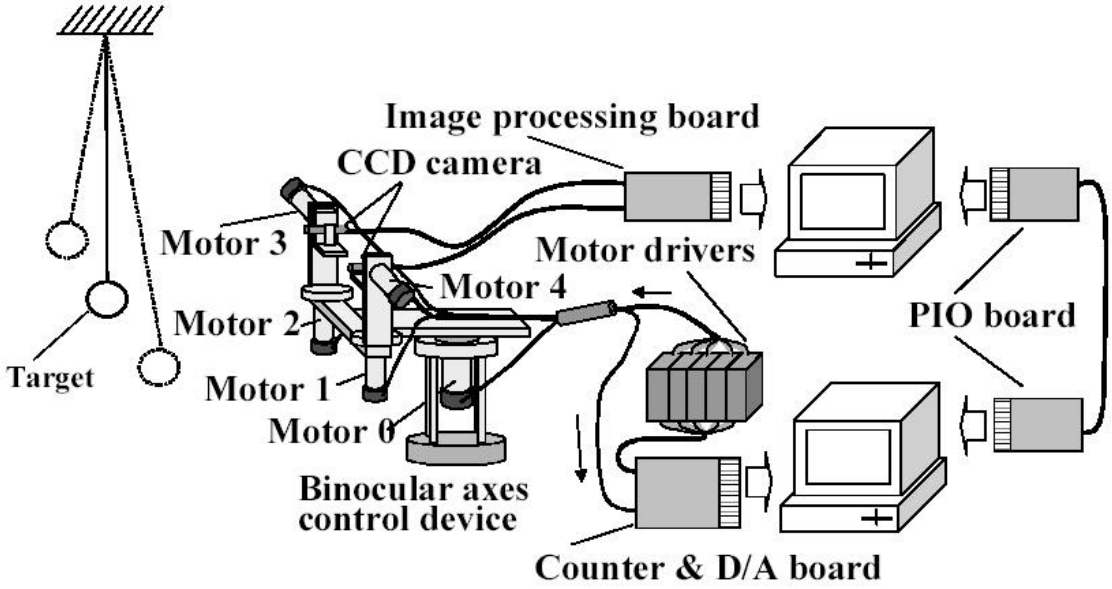

Fig. 10 Structure of robot eyes according to binocular motor system model

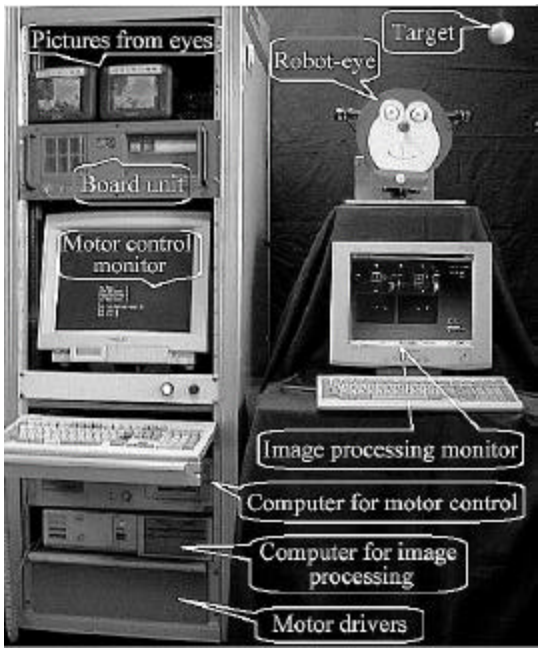

Fig. 11 Entire exterior of robot-eyes system

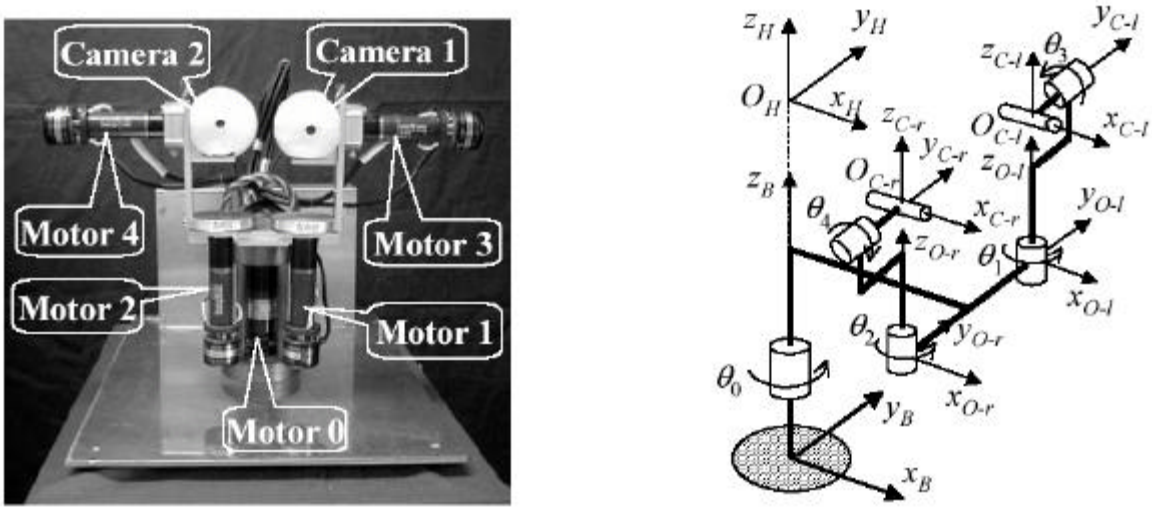

(a) Robot-eyes layout (b) Coordinate frames

Fig. 12 Structure of robot eyes

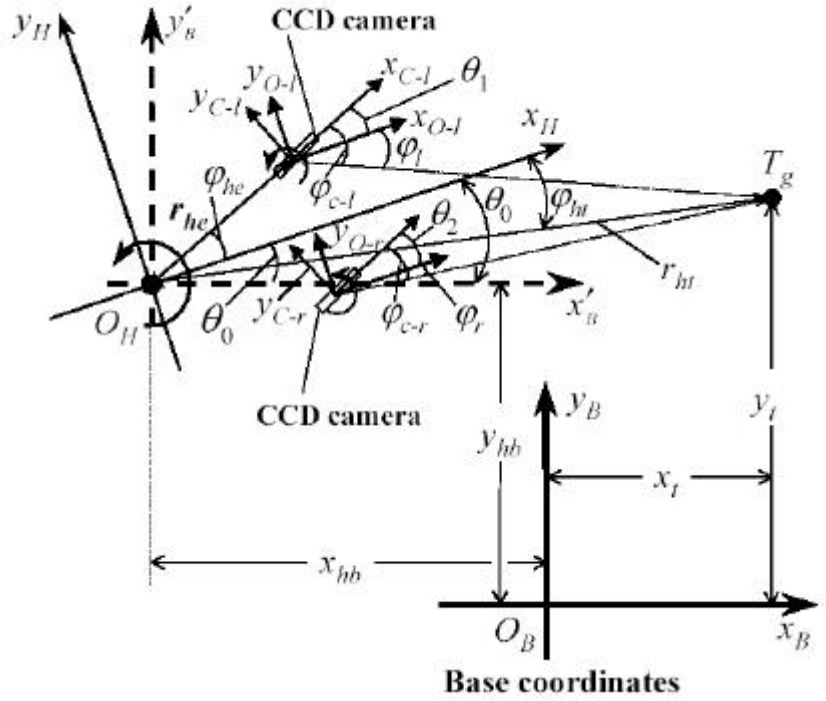

Fig. 13 Horizontal coordinate systems for robot-eye system

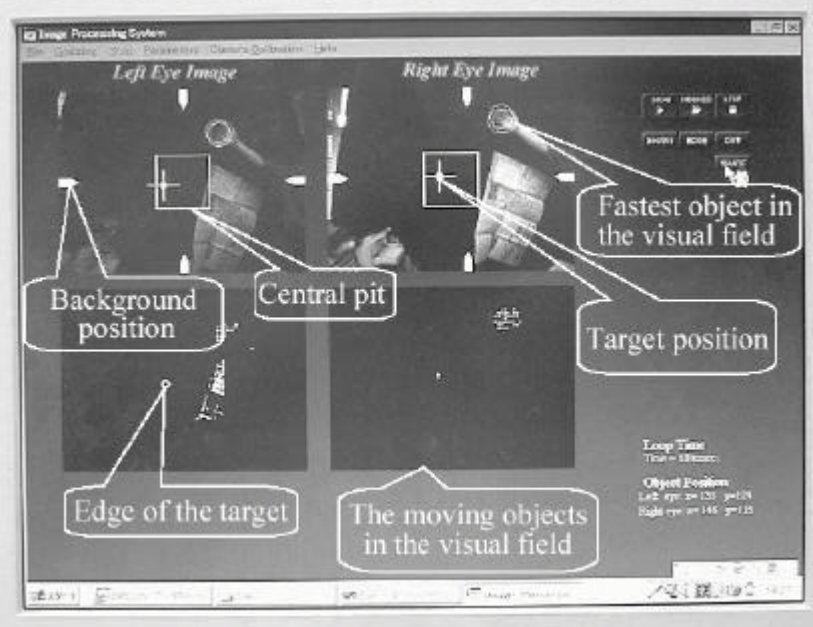

Fig. 14 The results of image processing

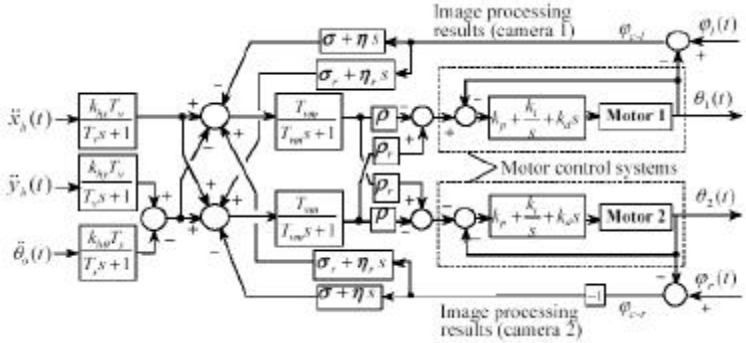

Fig. 15 Block diagram for robot-eye control system based on Fig. 9

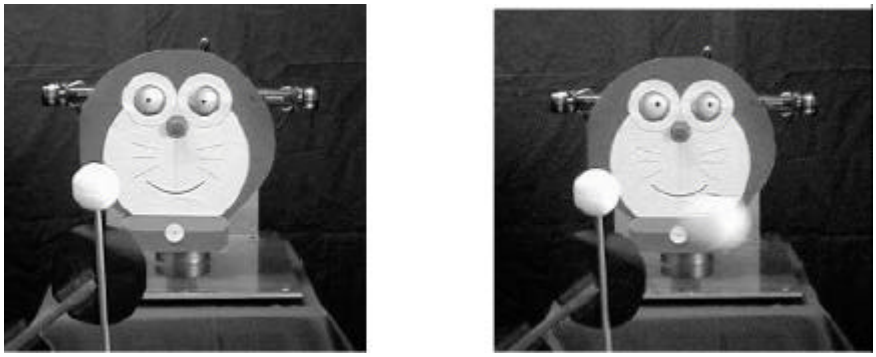

(a) Showing a first target (b) Showing the second target

Fig. 16 Circumstances of the experiments of same point gazing tendency.

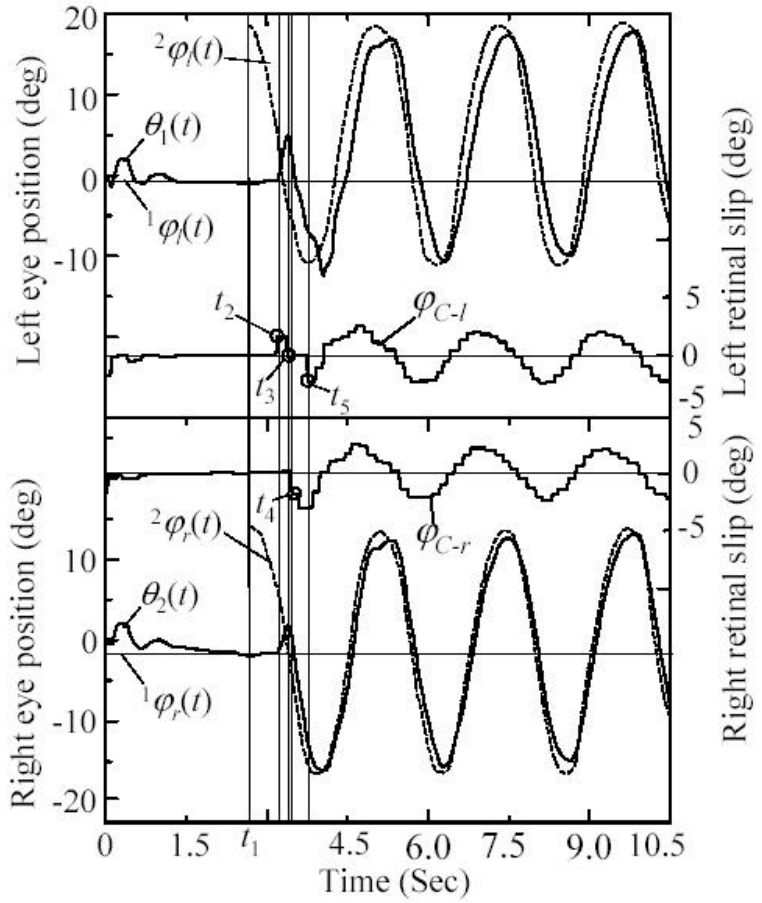

Fig. 17 The characteristic of eye movement by which two eyes gaze at only one target at the same time.

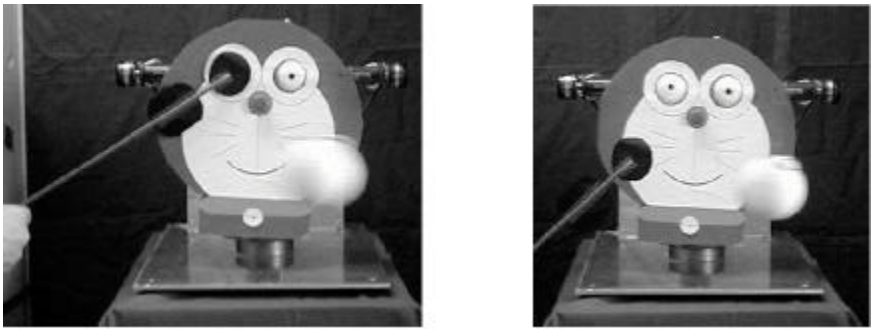

(a) Shutting the right eye (b) Taking off the obstacle

Fig. 18 The circumstances of the experiments of obstructing one eye.s view for a moment.

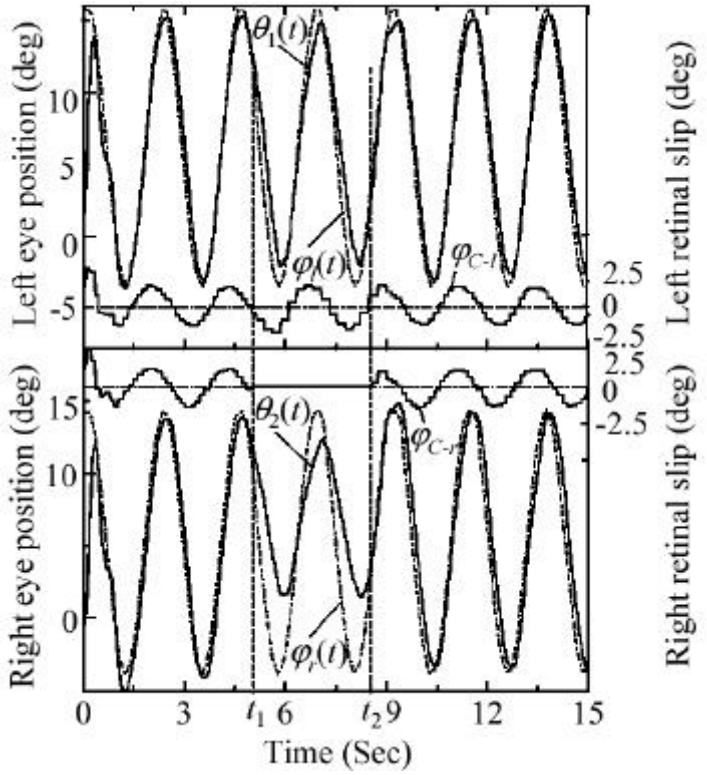

Fig. 19 Tracking of optic axes for smooth pursuit when the right .eye. was shut out in a term (t_1 to t_2).

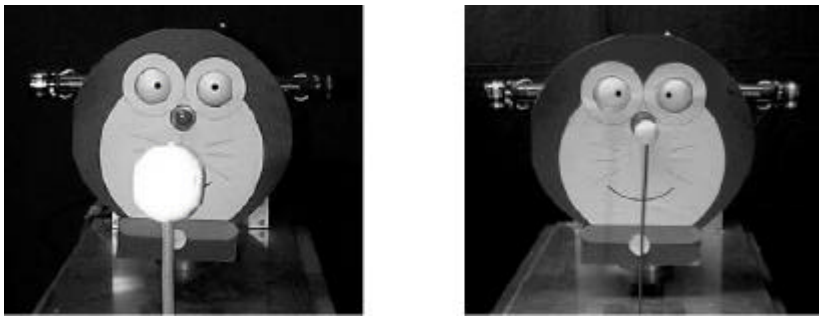

(a) (b)

Fig. 20 The circumstances of the experiment of vergence.

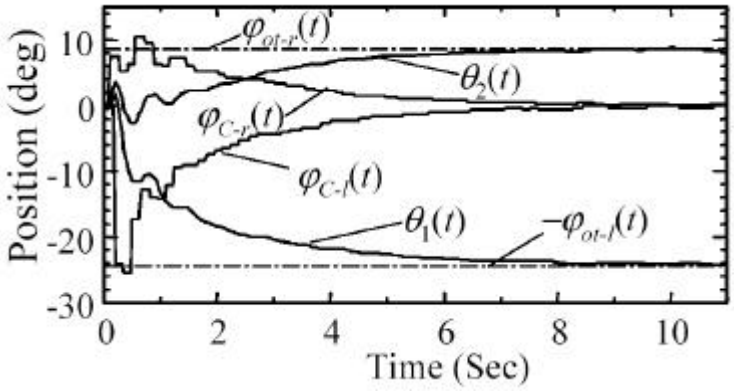

Fig. 21 Tracking of optic axes for vergence eye movement

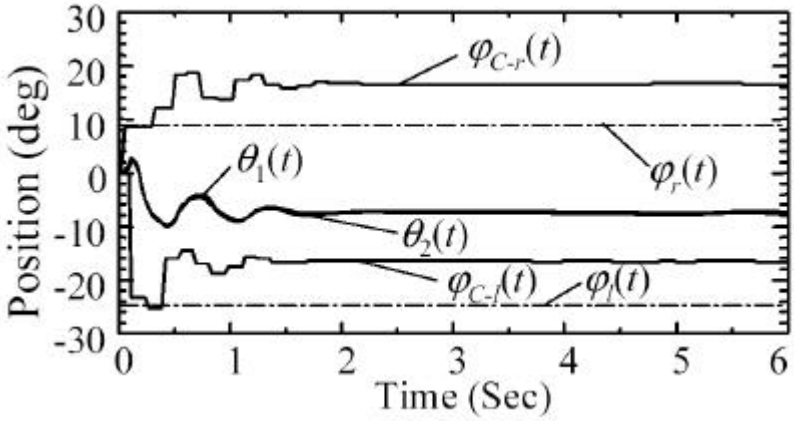

Fig. 22 Tracking of optic axes when $\tilde{n}_1 = \tilde{n}_2$.

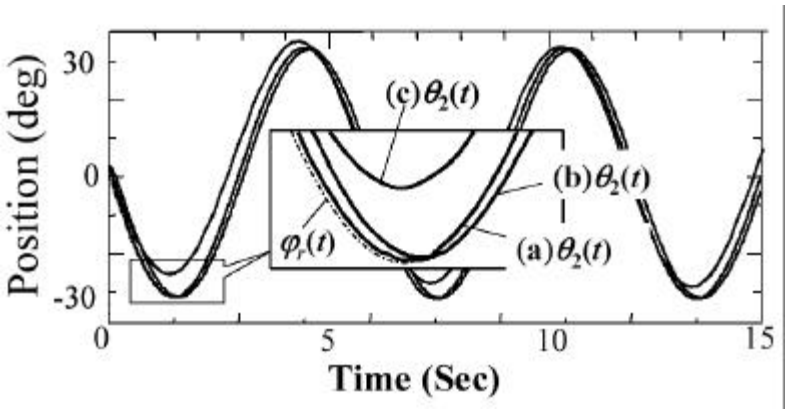

(a) Fixing target and rotating head,
(b) Fixing head and rotating target,
(c) Rotating head in a dark environment.
Fig. 23 Response of the binocular motor control system

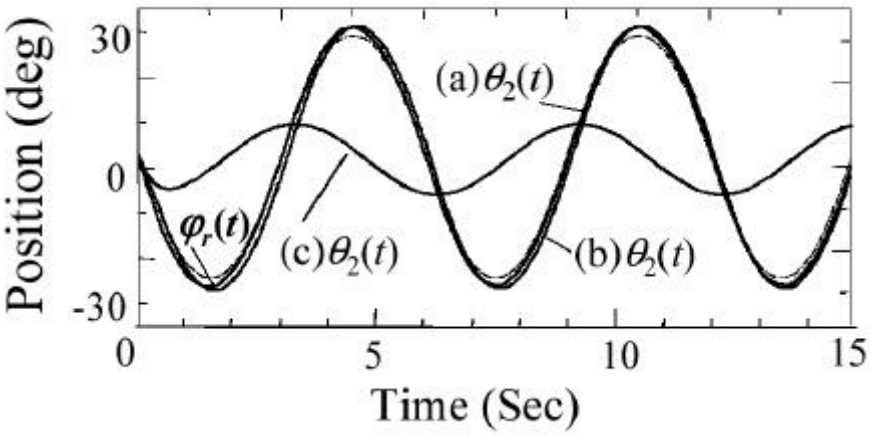

(a) Fixed target and moving head in y_H-direction,
(b) Fixed head and moving target in y_B-direction,
(c) Moving head in y_H direction in darkness.
Fig. 24 Response of the binocular motor control system

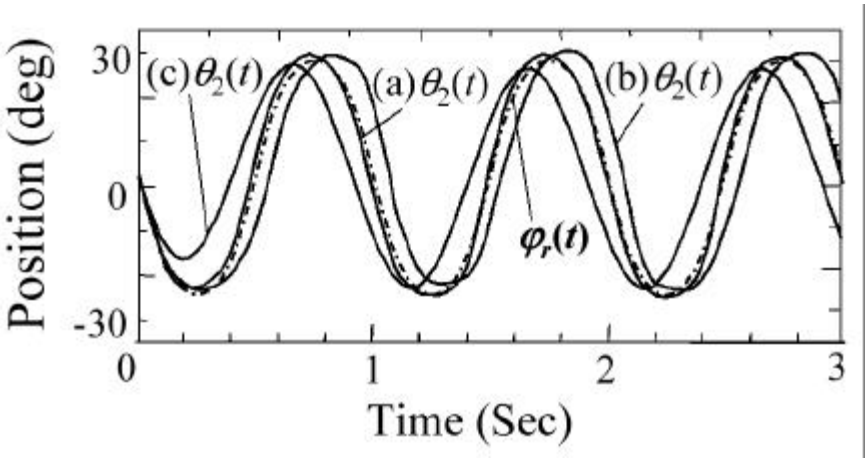

(a) Fixed target and moving head in y_H-direction,
(b) Fixed head and moving target in y_B-direction,
(c) Moving head in y_H direction in darkness.
Fig. 25 Response of the binocular motor control system

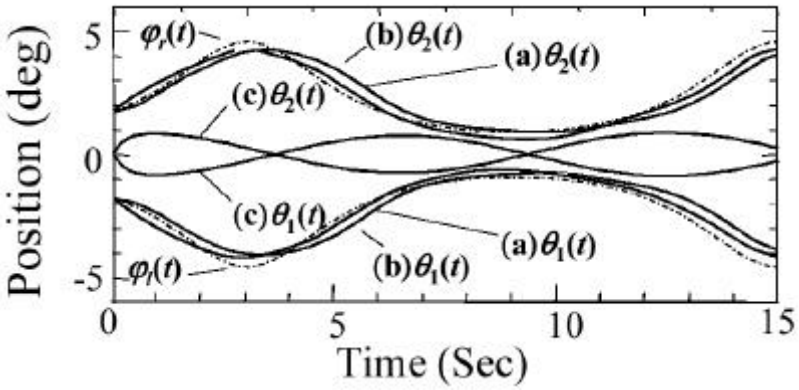

(a) Fixing target and moving head in *x*-direction.
(b) Fixing head and moving target in *x*-direction.
(c) Moving head in *x*-direction in darkness.
Fig. 26 Response of the binoc lar motor control system